THE MASSACHUSETTS INSTITUTE OF TECHNOLOGY

VARIABILITY IN SCORPIO X-1
A STUDY OF THE SCORPIO MONITOR EXPERIMENT ON SAS-3

A THESIS SUBMITTED TO THE FACULTY OF
THE DEPARTMENT OF EARTH AND PLANETARY SCIENCES
IN CANDIDACY FOR THE DEGREE OF

MASTER OF SCIENCE

BY

MICHAEL JOHN SCHOLTES

BOSTON, MASSACHUSETTS
MAY 1976

Certified by: Author's Signature: Accepted by:

—————————————   —————————————
Thesis Supervisor   Dept. Chairman

TABLE OF CONTENTS

LIST OF ILLUSTRATIONS

Figure

LIST OF TABLES

PREFACE

X-ray astronomy is an infant field, and SAS-3
(Small Astronomy Satellite #3, or Explorer 53) offers an enor-
mous and unprecedented opportunity for discovery. Fascinating
work has already been done using gas-filled proportional coun-
ters with rotation modulation collimators and narrow field slat
collimators, and a low energy system. Until now, little atten-
tion has been paid to the Scorpio Monitor Wide View Detector,
which was designed solely for three-channel observation of
Scorpio X-1. This analysis will examine the characteristics of
that detector and take a preliminary look at the data.

The author wishes to express his appreciation for the
advice of Professor Walter Lewin, Jeffrey Hoffman, and the
invaluable early work done by James Buff, Garret Jernigan, and
Ben Laufer. The author was greatly assisted in his questions
by John Richardson and John Nugent.

INTRODUCTION

The Scorpio Monitor Wide View Detector on the SAS-3 X-ray satellite is designed so that a relatively large amount of satellite time is spent with Sco X-1 in the field of view. This detector records three separate X-ray energy channels. The location of Sco X-1 is well known, and the Scorpio Monitor was designed with a very large field of view, since if the objective of observations is other than location of the source it is important to accumulate the maximum number of counts. The better the signal to noise ratio, the easier one can study time variability and spectral features. Precise physical mechanisms for the behavior of Sco X-1 are still not known, and thus careful observations of temporal variations and spectral changes are quite important. The Scorpio Monitor was built for precisely for this reason, and such observations of temporal variations are the object of this work.

To convert X-ray raw data to usable form, ie. to transform a number of counts observed per specific time bin into an apparent flux measured in keV cm^{-2} s^{-1} keV^{-1}, is a difficult process. One needs to know the aspect and geometry of the detector/collimator system at all times, as well as the physics of the X-ray interaction with the counter materials.

The data must be weighted to compensate for the best est-
imate of the response function and calibration. These steps
in the extraction of useful information will be examined
and demonstrated in the following chapters.

Before going into the properties of the detector, it
will be useful to review what is known and conjectured of
Scorpio X-1 for the purpose of later comparison.

Scorpio X-1 is widely variable in all energy regimes
and on all time scales at which it has been studied thus
far. The intensity variations can be divided into two
classes of behavior, quiescent periods of relatively little
activity and active periods with larger variations and occas-
ional flaring. A summary of observed variations is given in
Table 1, showing the intensity changes in all energy regimes,
the characteristic time scale of the change, and the typical
duration of such behavior.

In the radio regime, Sco X-1 is a triple source. The
highly variable central source lies at the position of the
optical star, and is flanked by two outer sources which are
separated by 1.2 minutes of arc. All three lie on a line
roughly parallel to the galactic equator. The central source
exhibits flaring behavior on a time scale of an hour. It is
flaring from 15 to 40 percent of the time, in a dormant or
steady-state condition approximately 25 percent of the time,

and continuously variable the rest of the time (about 60 percent) (Hjellming and Wade 1971, Wade and Hjellming 1971). There is some evidence of an H II region about one degree in extent around the central star.

Observations of infrared light from Sco X-1 indicate some kind of cut-off. The observed intensity is much lower than would be expected from a simple extrapolation of the X-ray spectrum.

At optical wavelengths the central source ranges from a B magnitude of 13.6 to 12.2, with a color index B-V= .23 (Neugebauer et. al. 1969). There is no Balmer discontinuity. There are active and quiescent periods, with flares of 0.1 to 0.2 magnitudes occurring only during active periods and when the source is brighter than B = 12.6 (Canizares et. al. 1975). There seem to be two or three preferred intensity states (Hiltner and Mook 1967, Canizares et. al 1975, Bradt et. al. 1975). The absolute intensity of the Hydrogen lines appears to remain constant as the continuum varies, making the line/ continuum flux ratios vary inversely with the B magnitude (Westphal,Sandage, and Christian 1968). The source changes color as it brightens, toward the blue (Mook 1967). Interesting low-excitation line features are seen at 4640 Angstroms, 4686 Angstroms, and 5696 Angstroms. The equivalent width of all three features increases monotinically with B magnitude (McClintock, Canizares, and Tarter 1975).

TABLE 1
OBSERVATIONAL CHARACTERISTICS OF SCORPIO X-1

Observer	Energy	Relative Intensity Change	Time Scale	Persistence
Hjellming & Wade 1971	radio	(flaring)	1 hr.	hrs. to days
Hiltner & Mook 1967	optical	350%	hrs to days	
Westphal, Sandage, & Kristian 1968	opt.	2%	1 min.	always
"		20%	1-10 min	hrs.
"		15%	30 min.	gradual ch.
Neugebauer & Oke 1969	optical	110%	3 hrs.	once
"		20%	3 min.	occasional
Evans et. al. 1970	X-ray	50%	2 min.	
Bradt et. al. 1975	X-ray	200%	6 min.	days
"		5%	min to hrs	days
Canizares et. al. 1973	X-ray	20%	4-20 hrs.	1-5 days
"		30-50%	30-40 min.	hrs to days
"		200-250%	30-40 min.	
"		100%	6 min.	once
Pelling 1973	X-ray	200%	hrs.	days
Lewin, Clark, & Smith 1968	20-30 keV	400%	10 min.	once
Agrawal et. al. 1969	30-50 keV		15 min.	

The 4686 Angstrom line has a central peak which changes its velocity relative to the main line. It has the maximum velocity at phase .25 of the .7873 day period and minimum velocity at phase .75. The peak is central at phase 0.0, and has a weak central reversal at phase 0.5 (Crampton and Cowley 1975). Maximum light occurs at the conjunction in which the emission object is most distant (Gottlieb 1974). The H lines and the He II line at lambda 4686 show inverse Doppler effects (Westphal, Sandage, and Kristian 1968). There is no optical polarization not attributable to interstellar effects(Mook 1969). There is evidence of H-beta emission from the sky near Sco X-1.

Whenever the source is active optically, it is also active in X-rays. The total X-ray luminosity is from 300 to 1000 times greater than the optical bolometric luminosity. No one-to-one correlation exists between X-ray and optical intensity changes. Although several coincident optical flares and enhanced X-ray emission have been observed, 1.5 hour delays have also been seen between an optical turn-on and an X-ray turn-on (Bradt et. al. 1975, Evans et. al. 1970). An optical turn-on and subsequent turn-off were observed, with no change in the X-ray intensity, which was in the quiescent state(Canizares et. al. 1975). X-ray flares show an intensity:hardness correlation; the flares are stronger at higher energies (Canizares et. al. 1975),

although in the hard X-ray region (greater than 20 keV)
the peak flare spectrum softens, approaching that of a
Planckian optically thick emitter with a maximum in the
main X-ray region (Lewin,Clark, and Smith 1968). There
is no X-ray bimodal effect, although there is a high int-
ensity tail on the brightness histogram (Canizares et. al.
1975, Pelling 1973). Flares occur in groups lasting about
four hours, and the pre- and post-flare intensity is near
the lowest quiescent-state value. No X-ray period is evident
from 6 min to 4 hrs. There does not appear to be any sys-
tematic correlation or delay between X-ray and radio var-
iations; Radio flares have been observed mainly while the
X-ray activity was quiescent. No X-ray line emissions have
yet been observed. Specifically, the equivalent width of the
Lyman-alpha line of hydrogenic sulfur at 2.6 keV is found
to be less than 2.2 eV, much less than expected(Kestenbaum,
Angel, and Novick 1971). There is no low energy cutoff at
.2 or .5 keV (Rappaport,Bradt, and Mayer 1969, Fritz et. al.
1968, Rappaport et. al. 1969).

A number of models have been proposed to explain this
fascinating variety of observational characteristics. Radial
velocity variations in the emission lines suggest gas stream-
ing or binary motion with a period of .7873 d, and are most
suggestive of binary motion when the source is quiescent
(Cowley and Crampton 1975). The presence of low-excitation
lines of He II, N III, O III, and C III implies temperatures

below 10^5 degrees Kelvin. The X-ray spectrum best fits an isothermal optically thin thermal bremsstrahlung process with a temperature of 6 x 10^7 degrees K(Chodil et. al. 1968). The hard X-ray spectrum implies temperatures near 2 x 10^8 deg. (Lewin,Clark,Smith 1968b). The lack of a Balmer discontinuity implies a continuum temperature above 10^5 degrees K.

The H-beta emission and possible H II region suggest either a stellar wind or X-ray ionization in the surrounding medium, or perhaps they are an effect of a previous nova mass efflux. In fact Scorpio X-1 much resembles an old nova or cataclysmic U Geminorum variable. The 4640 Angstrom line feature is rare in stars but appears in novae 3.5 mag below maximum light(Payne-Gaposchkin 1957). The UBV colors of the old novae are similar to Sco's. Such stars show large radial velocity changes, rapid flickering and minor outbursts, all similar to Sco X-1. The twin radio sources could be detritus from an old nova outburst. It is thought that nova behavior could be explained by mass accretion from a close companion.

A model has been suggested for Sco X-1 consisting of a secondary binary star overflowing its Roche lobe and dumping mass onto a white dwarf. The matter spirals down in an accretion ring, gaining thermal energy at the expense of gravitational potential energy via viscous drag. There will also be conductive heating of outer, cooler areas of the disk by inner, hotter ones. The IR and optical radiation

would come from an outer region of the disk at a temperature of 10^4-10^5 degrees K, and harder radiation would originate progressively nearer the surface of the dwarf. The peak lambda 4686 emission could originate in a hot spot on the following side of the accretion disk, with the main emission distributed all over the ring. From the velocity curve, the mass function $f(M) = (M_2 \sin i)^3/(M_1+M_2)^2 = 0.016$. Also, $a_1 \sin i = 6.3 \times 10^{10}$ cm (Cowley and Crampton 1975). The plasma emitting the X-rays would smear out any emission lines if it were dense enough ($n_e = 10^{16}$ cm^{-3}) for electron scattering to be important. A simple model in which all the emission originates in the same gas body has also been used with a limited degree of success to explain the source behavior. Kestenbaum et. al. 1971 estimates with this model that the optical depth in the visible region is around 5.9, due to the plasma density. Dense-plasma models explain the infrared and visual reduced intensities from what would be expected if the production mechanisms for X-ray and optical light were the same. Neugebauer et. al. 1969 has shown that the central radio emission can be explained by non-coherent synchrotron emission only if there is a mass flux outward. The supersonic thermal wind, which he finds plausible, could produce local H-beta emission and perhaps be responsible for the lateral radio source as well.

The lack of coupling between optical and Z-ray emission argues for at least partial separation of the emitting regions, a point which lends weight to the accretion disk model. The disk model can also account for falling optical intensity (Pringle and Rees 1972), and a fit to the spectrum of Sco X-1 can be achieved if $R(disk) = 10^{11}$ cm. From the orbital parameters derived by Cowley and Crampton, assuming an inclination angle of 15 degrees, the separation between the emission star and the center of mass is 2.4×10^{11} cm, in good agreement with the requirements of Pringle and Rees. One problem with the disk model is that the secondary has never been spectroscopically seen. By analogy with HZ Herc, the X-ray heating of the secondary should produce marked brightness changes. Either the primary is unusually bright or the secondary is fainter than expected for its radius. Unusual brightness could be due to high accretion rates. Unexpected faintness might indicate that the secondary is slightly evolved off the main sequence. For additional arguments in support of this last possibility, see Cowley and Crampton 1975.

Because of the highly variable nature of the source, it is often difficult to assign any one physical model which will completely explain the spectrum and time variations. It is crucially important that the observer not confuse instrumental effects for cosmic ones. The method of such discrimination shall now be examined.

I

THE DETECTOR

The Scorpio Monitor Wide View Detector consists of two small gas-filled proportional counters. The body of each counter is beryllium, 13 cm long by 4.45 cm wide by 2.03 cm deep, and the window is a 1 mil beryllium skin fronted by an open reinforcing grid called the strongback, which is 0.53 cm thick. The effective area of the two counters together is 25 cm^2. In front of the detector is a nickel-plated aluminum slat collimator 0.15 mm thick, which defines a field of view that is 12° by 60° full width at half maximum (FWHM). The center of the field of view lies in the yz plane of the satellite, elevated 30° above the y-axis. The long direction of the collimator is parallel to the satellite's equatorial plane.

The gas used to fill the counters is a mixture of argon, xenon, and carbon dioxide in the ratio 80:10:10, at a pressure of 1.3 atmospheres. The xenon serves to lessen the effect of the argon K-edge on the counter efficiency. Xenon and argon are the primary constituents because of the higher available gas gain and initial ionization of a monoatomic gas over a polyatomic gas; excitation of rotation and vibration states

are non-ionizing energy loss mechanisms which occur in a molecule but not in a noble gas. Also, the photoelectric cross section to 1-10 keV x-rays goes approximately as the fourth power of the atomic number, so the heavier the gas, the better. The reason for including carbon dioxide is that excited argon and xenon atoms emit ultraviolet light, to which they are transparent. Carbon dioxide absorbs this light, preventing it from striking the counter walls and starting a new multiplication sequence that would muddy the original pulse or be counted as a separate pulse, destroying the counter statistics. Also, argon and xenon can be excited to metastable states during the multiplication. They could then diffuse away from the vicinity of the anode wire and in decay, ionize an Auger electron which would register perceptibly later than the original event. Collisions with carbon dioxide de-excite the metastable atoms near the place and time of the original event, preserving the linearity between incoming photons and registering counts (Giacconi 1974).

There are three anode wires charged to a potential of 1500 volts, running longitudinally through each counter. A risetime discriminator in the onboard electronics eliminates slower-rising pulses caused by particle events, and high-level detectors sort the pulses into three energy channels.

The three channels are 1.0-2.5 keV, 2.5-5.0 keV, and 5.0-10.0 keV, which will be referred to throughout the rest of the paper as SCOA, SCOB, and SCOC, respectively.

The fisst major step in reducing the data is to determine the efficiency of the detector as a function of energy. In the simplest consideration, one must look at the transmission coefficients of the various materials comprising the detector. In addition to the mixed gas fill and the beryllium window, a thin thermal shroud covers the window. In order to be detected, a photon must traverse the shroud (aluminum and kimfoil) and the window, and be absorbed in the gas. The probability that this will occur is

$$\epsilon(E) = e^{-\mu_w X_w} e^{-\mu_{Al} X_{Al}} e^{-\mu_k X_k} \left(1 - e^{-\mu_g X_g}\right) \tag{1}$$

where ϵ is the efficiency, $\mu_{g(w,Al,k)}$ is the mass absorbtion coefficient of the gas (window, Al, kimfoil) in $cm^2 \, gm^{-1}$, and $X_{g(w,Al,k)}$ is the column density of the gas (window, Al, kimfoil) in $gm \, cm^{-2}$.

The mass absorbtion coefficient is energy-dependent and contains discontinuities at ionization edges. It can be expressed by the following relation.

$$\mu(E) = \rho \, 10^B \, E^A \tag{2}$$

The constants in Equation (2) are tabulated in Table 1.
For convenience, the mass absorbtion coefficient calculated
with these numbers will be in units of cm^2 per milligram,
so that the column densities can be left in units of mg cm^{-2}
in the calculation of the efficiency.

Another factor which affects the overall response of
the counter is the escape of x-ray energy due to the afore-
mentioned ultraviolet radiation from excited argon atoms.
This factor depends on the fluorescence rate of argon. The
argon K-edge is at 3.203 keV. When an x-ray of greater en-
ergy ionizes a K-electron the remaining energy can either
work to ionize other atoms, in which case it adds to the
multiplicative process and is not lost, or it can escape as
ultraviolet light. This appens only when the x-ray energy
was between 3.4 keV and 3.2 keV, the shell energy. More
energetic photons leave residual energies great enough to
ionize other electrons. For these counters the escape ratio
is 0.06 for E 3.2 keV and zero for E 3.2 keV, where the
escape ratio is defined as $Z(e)=$ the number of counts at an
energy $E-E_K$(shell energy) divided by the total number of
counts. Specifically, it is the number of counts from 0 to
0.2 keV excluding celestial photons in that range, divided
by the number of counts between 1.0 and 10.0 keV.

TABLE 2

TRANSMISSION CHARACTERISTICS OF DETECTOR MATERIALS

Material	E(keV)	ρ (gm cm^{-3})	A	B	χ(mg cm^{-2})	t(in.)
Be		1.80	-2.998	-0.24	5.84	0.001
Ar	$\leqslant$ 3.2	.00216*	-2.705	3.526	2.95	0.80
	> 3.2	"	-2.678	4.484	"	"
Xe	$\leqslant$ 4.783	.00714*	-2.059	3.810	1.44	0.80
	> 4.783					
	$\leqslant$ 34.55	"	-2.604	3.865	"	"
Al	$\leqslant$ 1.56	2.70	-2.751	4.973	0.016	(2000 Å)
	> 1.56	"	-2.735	1.191	"	"
Kapton $(C_{22}H_{10}O_5N_2)$	> .53	1.42	-2.838	0.389	0.36	.00014

*At 1.3 atm

More important than escape, however, is the effict on counter efficiency of the pulse shape discriminator. This electronic device is supposed to filter out slow-rising particle-background pulses, but in actuality it also filters out some of the x-rays. Its efficiency is defined as the number of x-ray counts which are not screened out divided by the total number of incoming x-ray counts. This mathematical function is poorly defined; it was determined experimentally at three discrete energies during pre-launch testing, and a parabolic fit to those three points is used as the continuous function $\epsilon_{PSD}(E)$. For the Scorpio Monitor, the efficiency of the pulse shape discriminator is defined as

$$\epsilon_{PSD} = -.00313\,E^2 + .0288\,E + .934 \tag{3}$$

In view of this equation, the expression for the net effective efficiency is

$$\epsilon(E) = e^{-\mu x_{Be}}\,e^{-\mu x_{K}}\,e^{-\mu x_{Al}}\left(1 - e^{-\left(\mu x_{Ar} + \mu x_{Be}\right)}\right)\left[-.00313E^2 + .0288E + .934\right] \tag{4}$$

and the expected count rate becomes

$$I = A \int_0^\infty \epsilon(E)\,\frac{dN}{dE}\int_{E_1}^{E_2} g(E,E')\,dE'\,dE \tag{5}$$

where $\frac{dN}{dE}$ = input spectrum

E_1, E_2 = energy channel boundaries

A = area

$$g(E,E') = \frac{1}{\sqrt{2\pi}(1+Z)}\left(\frac{Z}{\sigma_\lambda} e^{(E-E'-3.2)^2/2\sigma_\lambda^2} + \frac{1}{\sigma_B} e^{(E-E')^2/2\sigma_B^2}\right)$$

$$\sigma_\lambda = \frac{(.48/\sqrt{E-3.2})(E-3.2)}{2.354}$$

$$\sigma_B = \frac{(.48/\sqrt{E})E}{2.354} \qquad \text{(Matilsky 1975)}$$

Z = escape, .06 if $E > 3.2$, zero if $E < 3.2$

$.48/\sqrt{E}$ = energy resolution of the counter

In normal operation the energy band is resolved into three channels. Since ϵ_{PSD} has not been determined to greater accuracy, a sufficiently precise calculation of expected count rate can be done much more simply than in Equation (5). In illustration, start with the well known relation for the spectrum of the diffuse background above 1 keV, and let

$$\frac{dN}{dE} = 12.4 \, E^{-1.7} \, \text{photons cm}^{-2} \, \text{s}^{-1} \, \text{keV}^{-1} \, \text{ster}^{-1}$$

Evaluate this function at the average energy of the channel. Multiply by the effective area of the counter (25 cm^2), the effective solid angle of the field of view (.219 steradians) and the channel bandwidth. Finally multiply by the average efficiency of that channel in response to dN/dE, and the result is an expected intensity measured in counts per sec.

The average efficiency is just

$$\langle \epsilon \rangle = \frac{\int_{E_1}^{E_2} \epsilon(E) \frac{dN}{dE} dE}{\int_{E_1}^{E_2} \frac{dN}{dE} dE}$$

These calculations are summarized in Table 2.

The above calculations have assumed, as is normally done, the the source was centered in the field of view of the collimator. In actual operation the satellite is spinning, and the source describes an arc through the field of view of the detector. The count rate is proportional to the area of the window which is not in the x-ray shadow of the collimator. If the detector were oriented so that the view vector lay in the equatorial plane of the satellite, the response function would have a simple quasi-triangular shape:

$$R_o = \cos i \left(1 - \frac{\tan\theta}{\tan\theta_m}\right)\left(1 - \frac{\tan\varphi}{\tan\varphi_m}\right) \tag{6}$$

where R_o is the response $(0 \leq R_o \leq 1)$, i is the angle of incidence, φ is the longitude of the source in the detector, φ_m is the full width at half maximum in the long direction, ie. $60°$, θ is the latitude of the source in the detector, and θ_m is $12°$, the FWHM in the short direction (See Figure 1a).

TABLE 3

EXPECTED RESPONSE TO DIFFUSE BACKGROUND

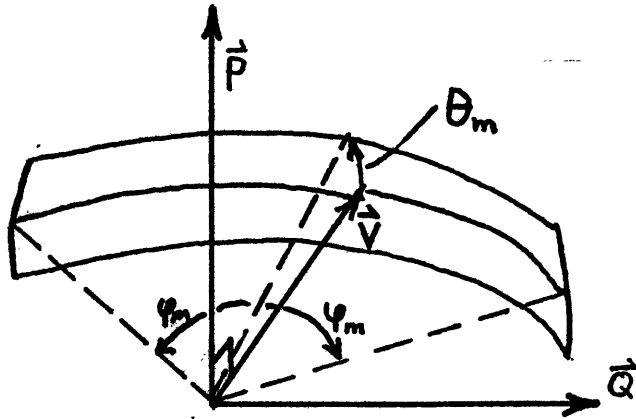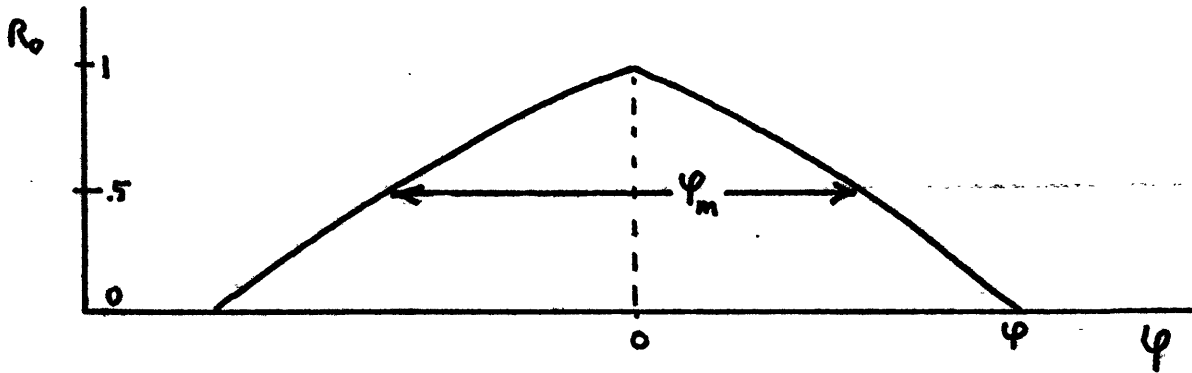| Channel	E(keV)	E_{ave}(keV)	ϵ_{eff}	$\langle \frac{dN}{dE} \rangle$	Solid Angle(ster)	ΔE	$A(cm^2)$	Expected BG(cts/s)
SCOA	1-2.5	1.75	.14	5.59	.219	1.5	25	6.4
SCOB	2.5-5	3.75	.78	1.434	.219	2.5	25	15.4
SCOC	5-10.0	7.5	.73	.441	.219	5.0	25	8.8

Fig. 1a. Field of View Geometry

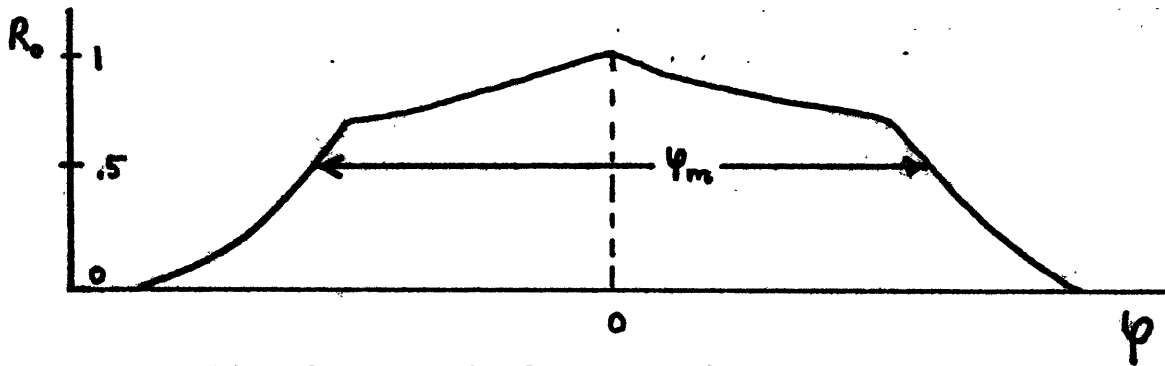Fig. 1b. Response of Unelevated Counter

Fig. 1c. Typical Sco Monitor Response

In the simple case described above, the angle θ would be a constant as long as the satellite's z-axis remained stationary, and the transmission as a function of φ would look very triangular (See Figure 1b).

However, when the detector center is elevated from the equatorial plane of the satellite, this simple picture no longer holds. To see this clearly, think of the limiting case, when the detector view direction equals the spin axis, or z-axis, of the satellite. Points in the sky describe circles through the field of view. The Sco Monitor has an elevation angle of 30° above the equatorial plane. As the satellite spins, points in the sky enter the field of view mostly at one edge and follow a gradual arc through it. If detector latitude is defined as the angle θ, the latitude of this arc is always changing, but the latitude of an arc at zero longitude ($\varphi=0$) is unique. Henceforth the phrase "latitude of the source in the detector" shall mean that the position of the source follows an arc through the field of view whose latitude at zero longitude is as stated.

Analytic expression of the response function (See Figure 1c) would be a mapping of spherical geometry onto the rectangular latitude-longitude geometry of the detector, and would be quite complex. In practise Equation (6) is

calculated for every data point, a much simpler process

than evaluation of an analytic solution would be. A more

convenient form of Equation (6) is

$$R_o = (\vec{S} \cdot \vec{V})\left(1 - \frac{\vec{S} \cdot \vec{P}}{\tan(\theta)(\vec{S} \cdot \vec{V})}\right)\left(1 - \frac{\vec{S} \cdot \vec{Q}}{\tan(\varphi)(\vec{S} \cdot \vec{V})}\right) \tag{7}$$

$\vec{S}$ is the source vector, $\vec{V}$ is the view vector, $\vec{P}$ is the

unit normal to the long collimator plane, $\vec{Q}$ is the unit

normal to the short collimator plane, and $\vec{S} \cdot \vec{V}$ is just the

angle of incidence (See Figure 1a).

Before launch, the satellite was mounted in an x-ray

calibration facility in which any detector could be illum-

inated by a narrow dispersion (12 arc seconds) broad band

x-ray beam. The satellite orientation could be shifted

to simulate various source positions. The results of

these ground calibrations were not entirely as expected.

The overall transmission as a function of φ and θ was

for the most part comparable to the expected value, but

some disturbing differences were manifest at negative

latitudes $(0 > \theta > -12°)$. There the response function be-

came horribly assymetric. A variable path length in air

(about a yard), which depended on the satellite orienta-

tion, separated the beam window from the detector. It

has been suggested that the air-path attenuation correc-

tions were in error. Since launch the detector has operated without any gross assymetries in its response to Sco X-1, the Crab Nebula, and other sources. Consequently the pre-flight calibration data has been rejected in favor of calibration with the actual x-ray data.

As previously stated, this data is on the whole quite symmetric about the point of zero longitude, which (for orbits when the latitude of the source in the detector is near zero) coincides with the maximum response. However, a number of geometric and structural effects cause the true response function to deviate from the one expressed in Equation (5) and Equation (6).

The first of these effects is that the column density of shroud, window, and gas is proportional to the secant of the angle of incidence, ie. $X = X \sec i = \frac{X}{\hat{S} \cdot \hat{V}}$. For detectors with narrow fields of view, this effect would be negligible, but for this detector, with a field of view 50°FWHM by 12°FWHM, it must be taken into consideration. The equation for detector efficiency is now

$$\epsilon(E,i) = \epsilon_{PSD}(E) \left(e^{-\mu X_{Al}} e^{-\mu X_k} e^{-\mu X_{Be}} \right)^{\sec i} * \left(1 - e^{-(\mu X_{Ar} + \mu X_{Xe})\sec i} \right) \tag{8}$$

where i equals the angle of incidence.
Numerical evaluation of Equation (8) is simplified by the assumption secant$(i) \sim$ secant(φ) . This assumption is

allowed, since for all of the data analyzed the latitude of the source in the detector was near zero. If one wished to generalize Equation (8) for any latitude, no such assumption would be allowed. Calculations of the efficiency as a function of energy and the angle φ are tabulated in Table 3.

One can see from these figures that as the angle of incidence increases, for energies below 5 keV the increased absorbtion in the window and thermal shroud dominates the increased efficiency of the gas, and the overall efficiency goes down. Above 5 keV the window and shroud are nearly transparent, and counter efficiency overall increases identically with gas efficiency. The net effect at the limiting angle of 50° is a 37% decrease in the efficiency of SCOA, a 10% decrease in the efficiency of SCOB, and a 14% increase in the efficiency of SCOC. Figure 2 is a plot of the counter response between one and ten thousand electron volts for longitude angles 0°, 25°, and 50°. Including this effect in the collimator response function given in Equation (6), the expected response is

$$R(E,\theta,\varphi) = R_{o}(\theta,\varphi) \, \frac{\epsilon(E,\theta,\varphi)}{\epsilon_{o}(E)} \qquad (9)$$

where R_{o} is the R_{o} of Eq.(6), ϵ is as given in Eq.(8), and $\epsilon_{o} \equiv \epsilon(E, \theta=0, \varphi=0)$.

TABLE 4

TRANSMISSION AS A FUNCTION OF ENERGY AND ANGLE

| φ Energy	0	10	15	20	25	30	40	50
1.0	0.0	0.0	0.0	0.0	0.0	0.0	0.0	0.0
1.75	.211	.206	.200	.191	.180	.166	.132	.090
2.0	.348	.343	.336	.326	.314	.297	.254	.195
2.5	.577	.572	.567	.558	.546	.532	.490	.429
3.0	.725	.722	.717	.711	.702	.691	.659	.609
3.75	.848	.846	.844	.840	.834	.828	.808	.775
4.0	.873	.872	.869	.866	.861	.855	.839	.810
5.0	.910	.911	.911	.911	.912	.911	.906	.894
6.0	.860	.862	.866	.871	.876	.883	.897	.908
7.0	.752	.756	.762	.770	.779	.792	.822	.857
7.5	.689	.693	.700	.709	.720	.734	.769	.812
8.0	.625	.631	.637	.646	.658	.673	.712	.763
9.0	.507	.512	.519	.528	.539	.554	.596	.653
10.0	.404	.409	.415	.423	.434	.448	.485	.542
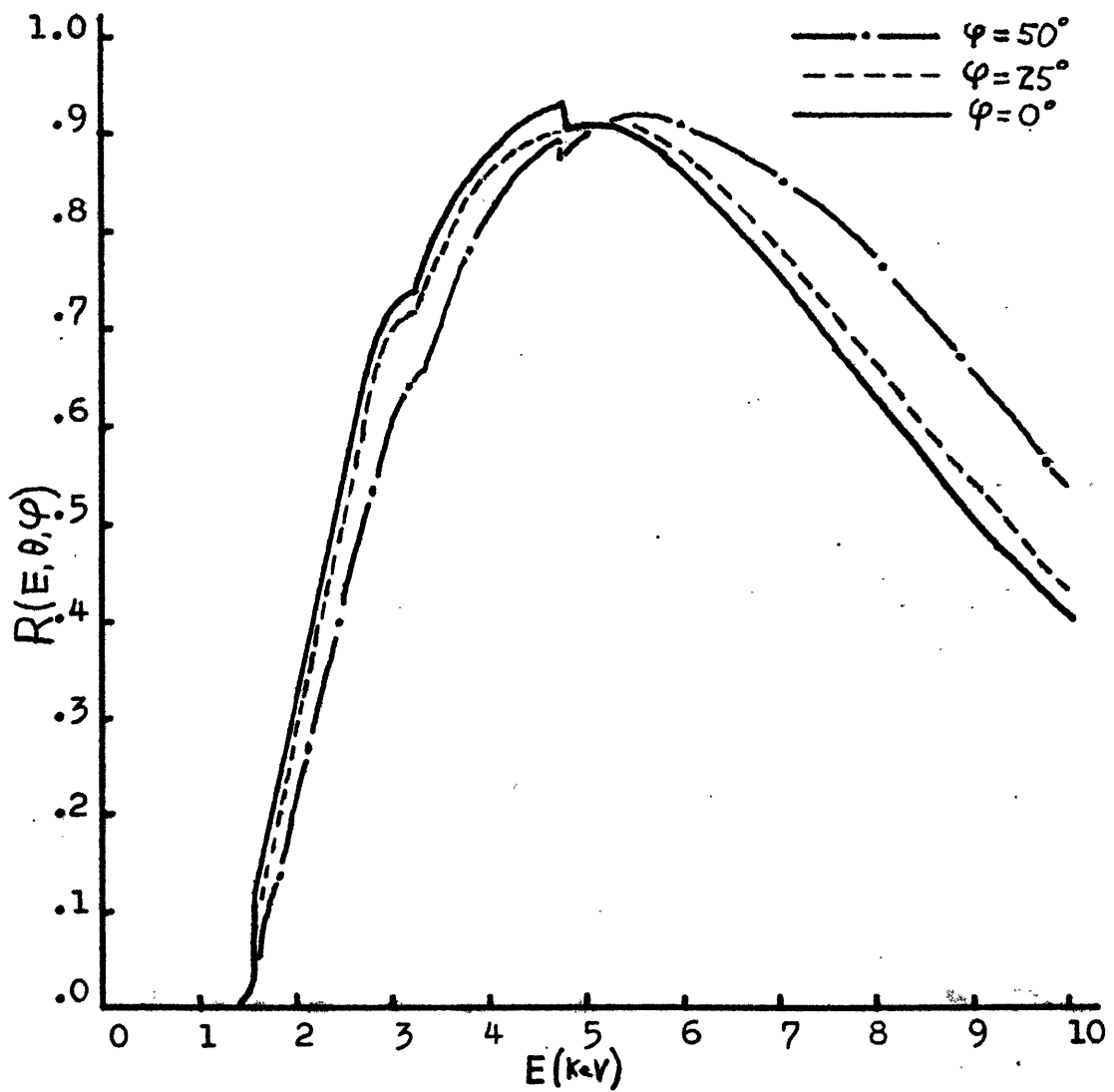
Fig. 2. Transmission Function at Different Angles

An additional perturbation on the collimator
response function arises in the physical construction
of the detector. The 1 mil beryllium window is fronted
by a relatively thick support grid called the strongback,
which prevents blowout of the 1.3 atmospheres internal
pressure and minimized risk of window damage during launch.
Each of the two counters is divided by the collimator into
four cells, two by two, and due to the strongback each
cell has five small windows of area .625 inch^2 apiece.
As the satellite spins, the x-ray shadow of the source by
the collimator travels the length of the cell and traver-
ses four strongback bars. When the shadow is traversing
a strongback, the amount of illuminated area is not
changeing. When a strongback is in the illuminated area,
the total response is a fractional portion less than one
would expect from an uninterrupted window, obviously.
The net effect of this geometry is the occurrence of four
ledges in the response function on each side of the center.
Figure 3a portrays the surface of a cell (there are eight
cells in all), Figure 3b shows the deviation of the trans-
mission function from $R_o(\theta, \varphi) \left(\equiv R_o(time) \right)$ as a result of the
strongback effect, and Figure 3c shows the deviation from
R_o due to the secant law, from Table 4.

This effect is only mildly dependent on energy,
since the strongback thickness of .209 inches renders it

virtually opaque over the entire energy band of the detector. The strongback exerts another effect on the response function because its finite height (.53 cm) casts a shadow at non-zero longitude angles. The expression for the height of the ledges in Figure 3b is

$$\frac{1}{\ell}\left(h\tan i + S\right)\overline{\left(1 - \frac{\tan i}{\tan i_m}\right)} \quad ; \quad i_m = 56° \tag{10}$$

where ℓ is the cell length (6.59 cm), h and S are the strongback height and width, and i is the angle of inclination of the shadow edge which intercepts the strongback. The total deviation from the non-strongbacked cell response as a function of i is

$$D(i) = \left(\frac{h}{\ell}\tan i + \frac{S}{\ell}\right)\overline{\left(1 - \frac{\tan i}{\tan i_m}\right)}\sum_{j=1}^{5} \mathcal{U}(i - i_j) \quad ; \quad i_m = 56° \tag{11}$$

where D is the deviation. $\mathcal{U}(i - i_j)$ is defined as zero for angles of inclination $i > i_j + \Delta i_j$, one for angles $i < i_j - \Delta i_j$, where i_j is the angle from the j th strongback to the edge of the collimator, Δi_j is the angular width of the strongback at angle i_j , and $\mathcal{U} \equiv \frac{i - i_j + 2\Delta i_j}{2\Delta i_j}$ if $i_j - \Delta i_j \leqslant i \leqslant i_j + \Delta i_j$. The final form of the response function is

$$R(E, \theta, \varphi) = R_o(\theta, \varphi) \frac{\epsilon(E, \theta, \varphi)}{\epsilon_o(E)} \left(1 - D(\varphi)\right) \tag{12}$$
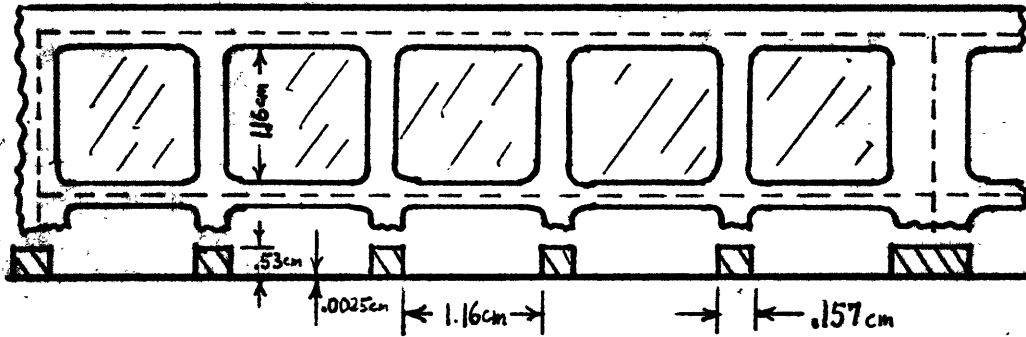
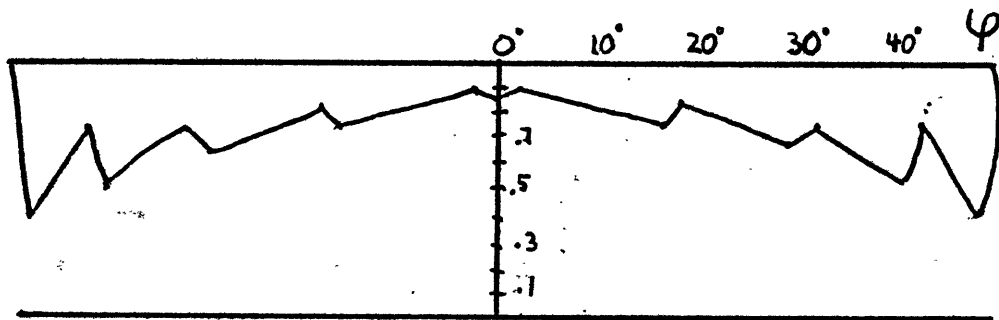**Fig. 3a.** Face-on and Side Views of the Strongback

Fig. 3b. Effective Efficiency Due to Strongback

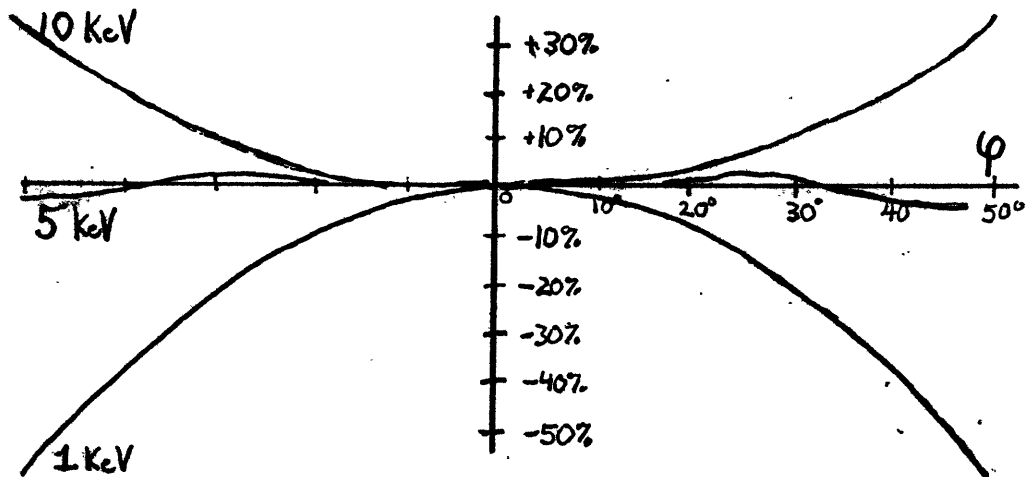**Fig. 3c.** Effect of Secant Law on Response Function

and the simplified form which neglects variations in R.
due to changes in θ is

$$R(E,\theta,\varphi) = \cos[i(\theta,\varphi)]\left[1 - \frac{\tan\theta}{\tan\theta_m}\right]\left[1 - \frac{\tan\varphi}{\tan\varphi_m}\right] \cdot$$

$$* \frac{\exp[-(\mu x_{Be}+\mu x_{\kappa}+\mu x_{Al})\sec\varphi]\left[1 - e^{-(\mu x_{Ar}+\mu x_{\kappa e})\sec\varphi}\right]}{\exp[-(\mu x_{Be}+\mu x_{\kappa}+\mu x_{Al})]\left[1 - e^{-(\mu x_{Ar}+\mu x_{\kappa e})}\right]}$$

$$* \left[1 - \frac{1}{\lambda}\left(h\tan\varphi + s\right)\frac{1}{\left(1 - \frac{\tan\varphi}{\tan\varphi_m}\right)}\sum_{j=1}^{s} U(\varphi - \varphi_j, s)\right] \tag{13}$$

There is a simple way to avoid this calculation.
The raw x-ray data is divided by $R_0(\theta,\varphi)$ to derive a source
intensity. If R_0 is the true response function and the
source is constant, the derived intensities of all the
data points will be the same. However, if R_0 deviates
from the true response function, the calculated intensity
will deviate inversely. That is, if R_0 is higher at a
given time than the true function, the intensity will be
lower than its true value, and vice versa. By looking
at the deviations of the derived apparent intensities
from a constant value, one can obtain a measure of the ex-
tent to which the function R_0 deviates from the true res-
ponse function. R_0 can subsequently be multiplied by a
factor which changes it as much as is necessary to make
the derived intensities all constant. The range of φ
is divided up into intervals, and the discrete factor
for each interval is stored in a table or file which can

be accessed by the computer program which computes $R(E,\theta,\varphi)$.
For example, if the derived intensity using $R_0(\theta,\varphi)$ is a ,
and the true intensity is b , the factor to be stored is
just a/b . $R_0(\theta,\varphi)$ times this number, which is assigned to
a specific interval of φ , should equal the true response.
Calibrating thus eliminates the laborious theoretical
calculations and their measurement uncertainties. In the
short collimator direction the simple case is assumed, and
in the long direction nothing is calculated--the data it-
self determines the true response function.

Care must be exercised in choosing the calibration
source, since the response function will depend on the
spectrum of the source. It is best to recalibrate for
each source. Complications arise when one tries to
calibrate using Sco X-1 data. The true intensity is highly
variable, and using the procedure described above one could
derive an adjusted response function which was adjusted not
for errors in the test response function, but for the ran-
dom intensity variations of the source during the cali-
bration orbit. An attempt was made to eliminate the ran-
dom variations by superimposing the data from many orbits,
which would make random variations tend to destructively
interfere, and would allow the systematic variations to
constructively interfere. Data for fifteen orbits over
a six day period was superimposed, with limited success.
Systematic errors in the response function still exist.

Many more orbits would have to be superimposed to improve
the statistics of the random element elimination. At this
time it would seem that creating a similar table contain-
ing the theoretically derived quantities $\frac{\epsilon(E,\theta,\varphi)}{\epsilon_\alpha(E)}\left(1 - D(\varphi)\right)$
would be more likely of success. And if systematic dev-
iations persist, due to some forgotten element of the
true response function, it will be a simple matter to
adjust the table of factors in compensation.

II

THE OBSERVATIONS

The SAS-3 satellite was designed so that whenever observations were being made of the galactic center region using the pole slat collimated detectors, or more specifically whenever the pole of the satellite was near the galactic north pole, Scorpio X-1 would be visible in the Scorpio Monitor Wide View Detector. The satellite has been used in this way a great deal since launch in May of 1975, and consequently there is much data available on Sco X-1. It was not difficult to find a sequence of orbits in which the latitude of Sco X-1 in the detector was near zero, and these orbits were chosen for the first analysis in order to minimize the size of corrections which would have to be made in the theoretical transmission function. The twenty-two orbits chosen cover a six day period of time from Julian Day 2,442,794.34 to JD 2,442,800.66. The latitude of the source in the detector varied from -4.4° to $+2.81^{\circ}$, although nineteen orbits were between -1.0° and $+2.0^{\circ}$. The quality of the data was good; in all cases there was less than 10% of the data lost in dropouts, and in no case was the satellite near

the South Atlantic Anomaly at the time of the source tran-
sit. In eight of the orbits the source went into earth
occultation after from 14 to 28 minutes of good data had
been collected. Occultation does not affect the reliabil-
ity of the un-occulted intensities. The satellite was
spinning at one revolution per orbit, and a transit of the
source through the field of view had a typical duration of
29 minutes, compatible with the collimator full width of
112 degrees. The data was collected in bins of 1.66285
seconds and stored on tape.

III

THE INITIAL REDUCTION

The first step in the data subtraction process was subtraction of the background, which was determined by a time average of the signal when the source was not in view. This background was typically 29.3 cts/bin, or 17.6 cts/sec, from 1.0 to 2.5 keV; it was 23.6 cts/sec from 2.5 to 5.0 keV; and it was 17.7 cts/sec from 5.0 to 10.0 keV. This level of background is significantly higher than that predicted using Equation (5) and the relation for diffuse count rate $dN/dE = 12.4 \, E^{-1.7}$. The difference corresponds to the rather large noise rate of 22 counts per second in each channel, attributable to the electronics.

The next step in data reduction was to calculate an expected flux, a template, for each bin, using the simplest collimator response function as given in Equation (6). The difference between the raw data and the background was divided by this template value to yield an apparent flux. The variations in the derived apparent fluxes were similar in each orbit, indicating systematic errors in the response function. It was assumed that the

average apparent flux was comparable to the true flux, or equivalently that the systematic errors balanced on the whole. The average was divided by each apparent flux to yield a number which, when multiplied by the template would give an adjusted template. A test was made in each case to see that the adjusted template actually made the apparent fluxes equal the average.

Finally, when an adjusted template had been formed for each of the orbits under consideration, all the templates were averaged together. As previously stated, it was hoped that variations in the templates due to temporal changes in Sco X-1 would, for the most part, cancel out on the average.

Each orbit was then re-analyzed using the cumulative template, which was resolved into a table covering the range of φ and the function R_0. The template represents the collimator response and counter efficiency over a range of φ from approximately $-56°$ to $+56°$, which is the full width of the field of view.

Once a file of correlated intensities and times had been created, secondary data reduction procedures were followed.

A fast Fourier transform on selected portions of each orbit was performed over the frequency range 0.04 Hertz to

0.62 Hertz. No statistically significant power densities were observed in any orbit. The only semi-recurrent feature in the power density spectrum was a region of slightly higher density corresponding to characteristic periods of 7 to 12 seconds. No interpretation of its importance, if any, can be made at this time.

In examining the derived apparent fluxes for Sco X-1, at first glance the data seems to be of poor quality. The magnitude of variations which are clearly systematic errors in some cases approaches fifteen percent, and the behavior of the answers at large magnitudes of φ is highly erratic. To a certain degree that behavior was expected, since the low count-rate at those angles means that random errors and background fluctuations are greatly multiplied when the raw data is divided by the template, a very small number. Other errors can be traced to accidental positive reinforcement of real light variations in Sco X-1, and the resulting inaccuracy of the template. It should be possible to select orbits in which Sco varies very little, and which, when averaged, would have better results. It would also be possible to consider the nature of the systematic errors and change the template table a bit at a time until they disappear. However, considering the hit

or miss nature of this procedure, the best method of forming an accurate template appears to be brute force calculation via Equation (12).

In this analysis, using the cumulative template, moderately reliable fluxes are derived for angles between plus and minus 30°, with less than 5% systematic errors. Although serious analysis should await the perfection of the response function, it is possible to do some meaningful analysis of absolute fluxes and spectral properties.

The first such analysis was the creation of a light curve over these twenty-two orbits. It is possible to see non-spurulous intensity variations on a scale of 0.1 and 0.3 days, with a magnitude of from five to twenty percent. No variations larger than twenty percent were observed. An attempt was made to correlated the light variations to the established .78 day period of Sco X-1. Results are inconclusive. No periodic variation could be established, but not enough orbits had been analyzed to give a useful limiting amplitude, and the spread of the erratic high φ values is so great in each orbit that it become difficult to pick out a mean intensity for the orbit. An absolute calibration will be necessary before the derived intensities can be trusted. A first

attempt at absolute calibration was made using the spect-
rum of the Crab Nebula. Theoretical expected count rates
were derived by folding the spectrum of the Crab against
the response function of the detector. The predicted count
rates are 41.8, 34.17, and 11.69 cts/sec in SCOA, SCØB,
and SCOC respectively (Li 1976). The Crab was observed
at Julian Day 2,442,767.9 , and correcting for the fact
that the latitude of the source in the detector was -2.53°,
count rates of 40.65, 29.63, and 13.22 were observed in
the three channels. The agreement is close enough to war-
rant using Sco X-1 data as is, although it should be pos-
sible to arrive at a more satisfactory expression for
ϵ_{PSO} using these two sets of numbers.

Using the Sco X-1 data as it is, one count per sec-
ond corresponds to .285,.051, and .055 photons $s^{-1} cm^{-2}$
in SCOA, SCOB, and SCOC. This corresponds to an energy
output by Sco X-1 of 10^{35} erg $s^{-1}(r/500$ pc$)^{2}$, which is
reasonable, since typical count rates over all channels
are 10^{3} counts per second and the source has a luminosity
of 10^{37} erg s^{-1}. A more quantitative analysis would require
folding the spectrum of Sco X-1 with the detector response
function to get accurate effective efficiencies.

Another qualitative look at the data which was per-
formed was a correlation between the total intensity of

the source and the ratio of two channels, ie. a hardness
plot. If intensity is plotted against the ratio of SCOA
to SCOB, the locus of points moves toward lower ratios
as intensity increases. That is, the source gets bluer
as it gets brighter. This effect is expected is the
source spectrum looks something like an exponential in
the form $\exp(-k/T)$, where k is the x-ray energy, and
T is temperature. As T increases (system gets bluer)
$\exp(-k/T)$ also increases, ie. the same energy k is as-
sociated with a higher intensity. The locus of inten-
sity versus SCOB/SCOC is essentially vertical; SCOB
over SCOC is largely constant. This could be due to
the fact that above 3 keV the spectrum is slowly varying
compared to below 3 keV, and the blueing effect is just
too small to see in the tail of the exponential spectrum.

Color-color plots were also made from the data in
these twenty-two orbits. The most noticeable feature of
these plots is that the points cluster along a straight
line passing near the origin which is sharply defined
for SCOA vs. SCOB and SCOB vs. SCOC, but less well defined
for SCOA vs. SCOC. That the locus of points approximates
a straight line is an indication that the source spectrum
is fairly simple and quite similar at the energies involved.

When the slope of the color locus changes, another component of the spectrum is coming into dominance. By examining the slopes of these lines one should in theory be able to tell something about the form of the spectrum. For such a problem, however, an accurate response function is essential, since the scatter of points due to systematic errors makes determination of the color locus more difficult.

A final correlation made on the data was a histogram of intensities versus the number of times those intensities were observed. For all the channels the result is a well defined distribution very much like a Poisson distribution, with the main difference being that the standard deviation is much larger than one would expect from a Poisson process. The broadening is due to variations in source intensity and response function systematic errors. The mean count rate for those twenty-two orbits was 320 cts/sec in SCOA with sigma = 60 cts/sec, 260 cts/sec in SCOB with sigma = 70 cts/sec, and 90 cts/sec in SCOC with sigma = 50 cts/sec. As a point of comparison, sigma for a Poisson distribution at 320 cts/sec would be 24 cts/sec. For examples of a hardness plot, a color plot, and an intensity histogram for the 22 analyzed orbits (1030 data points) see Figures 4 - 12.
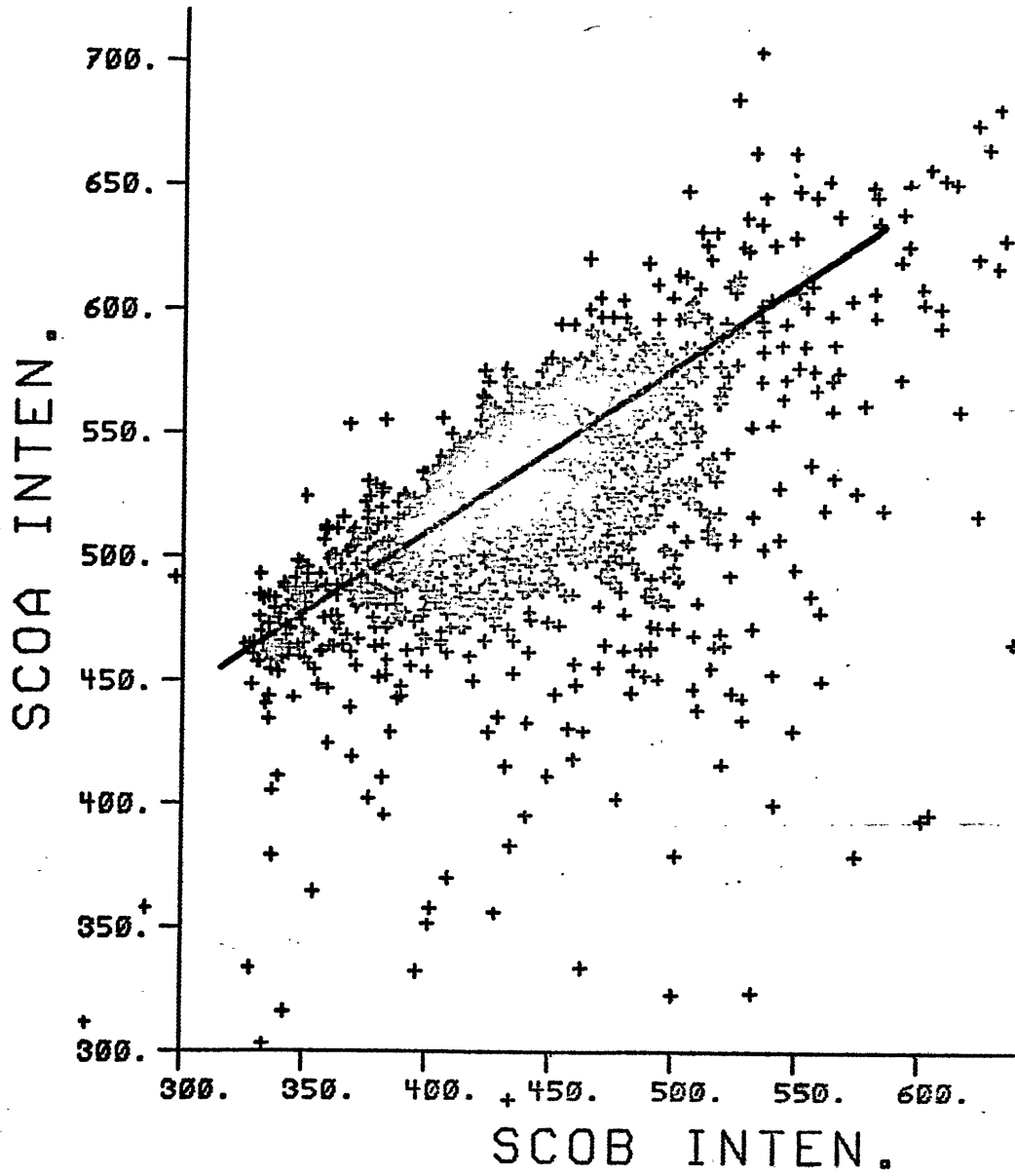
Fig. 4. 1.75: 3.75 keV Color-color Plot.
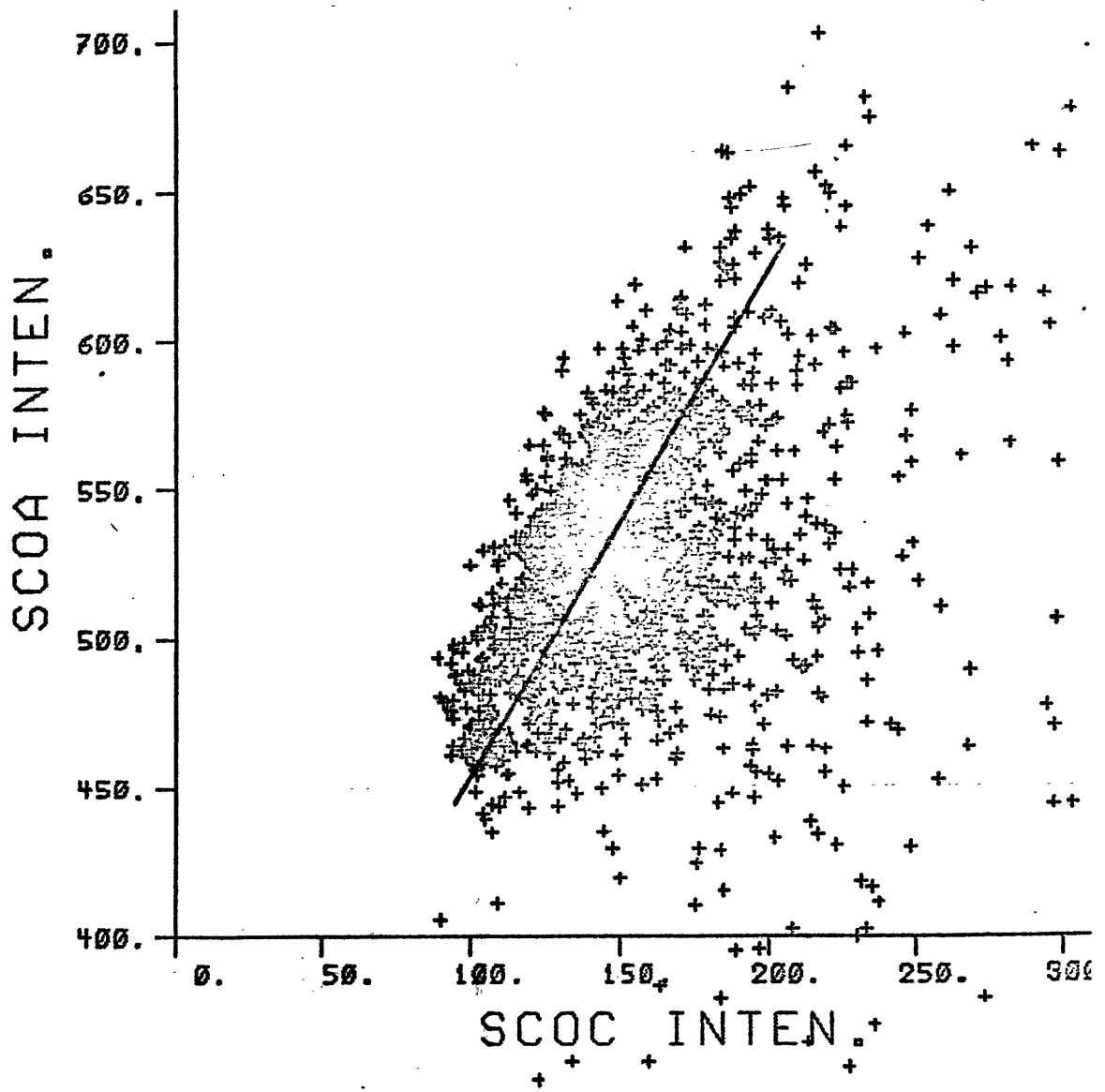
Fig. 5. 1.75: 7.5 keV Color-color Plot.
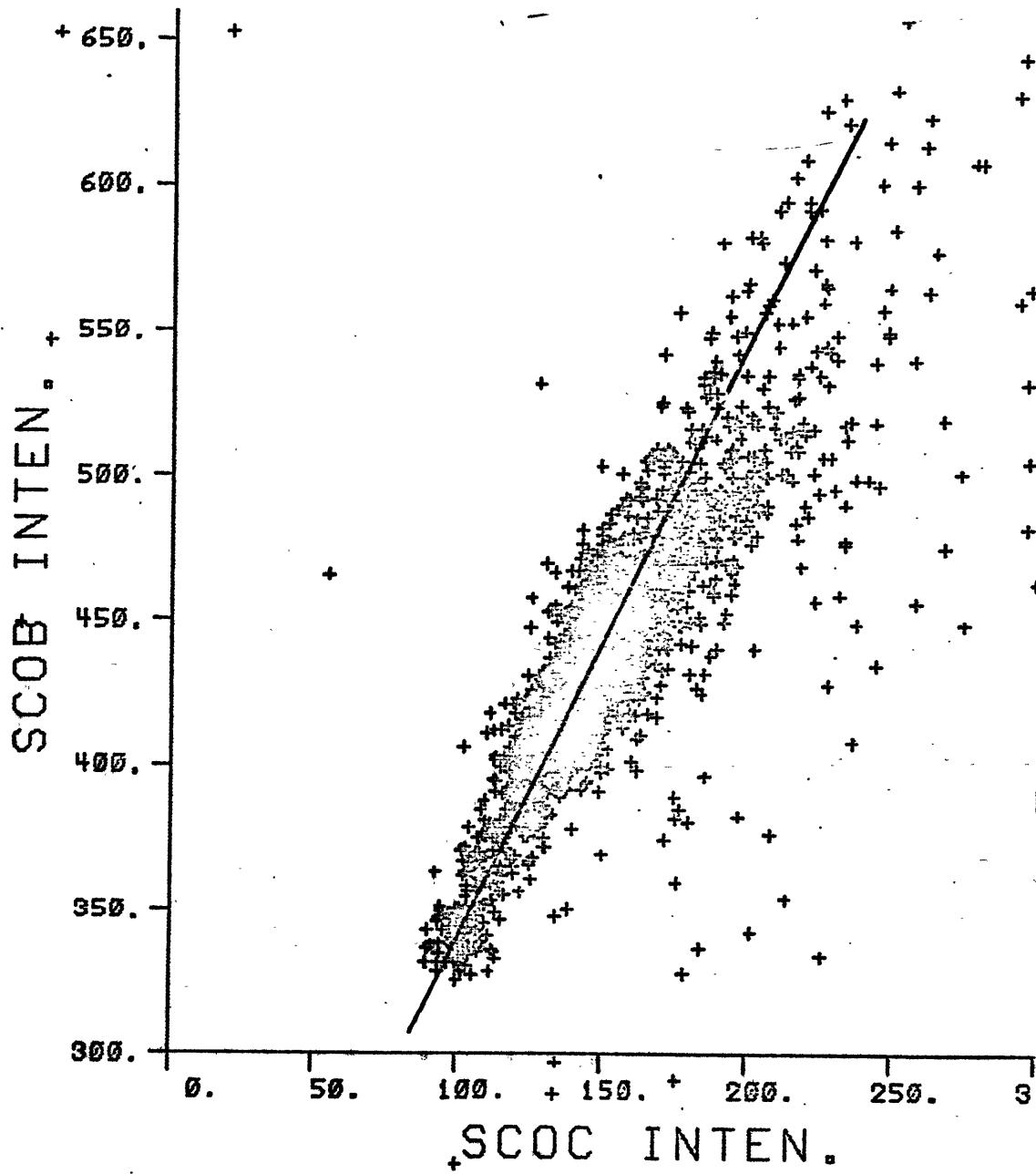
Fig. 6. 3.75: 7.5 keV Color-color Plot.

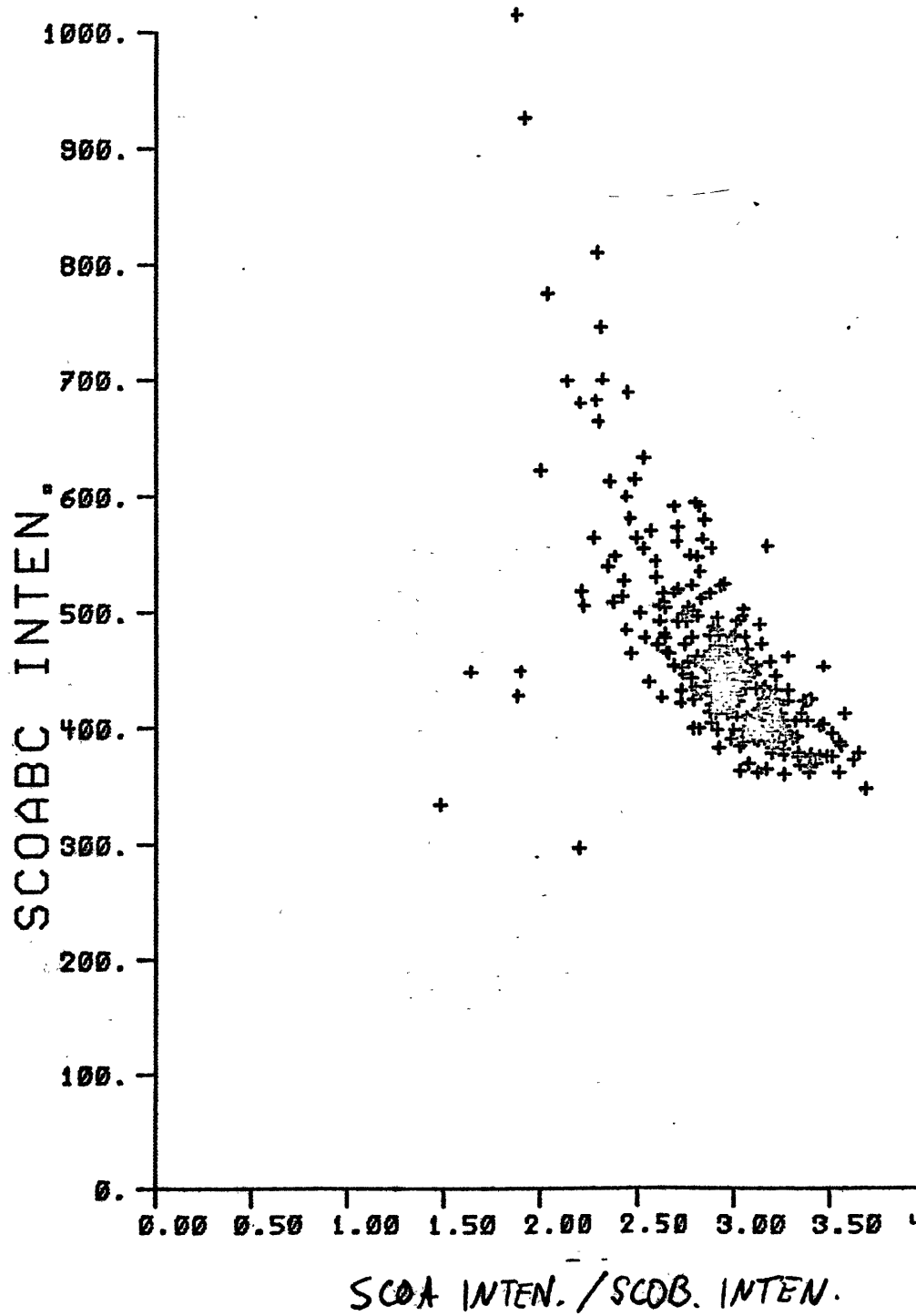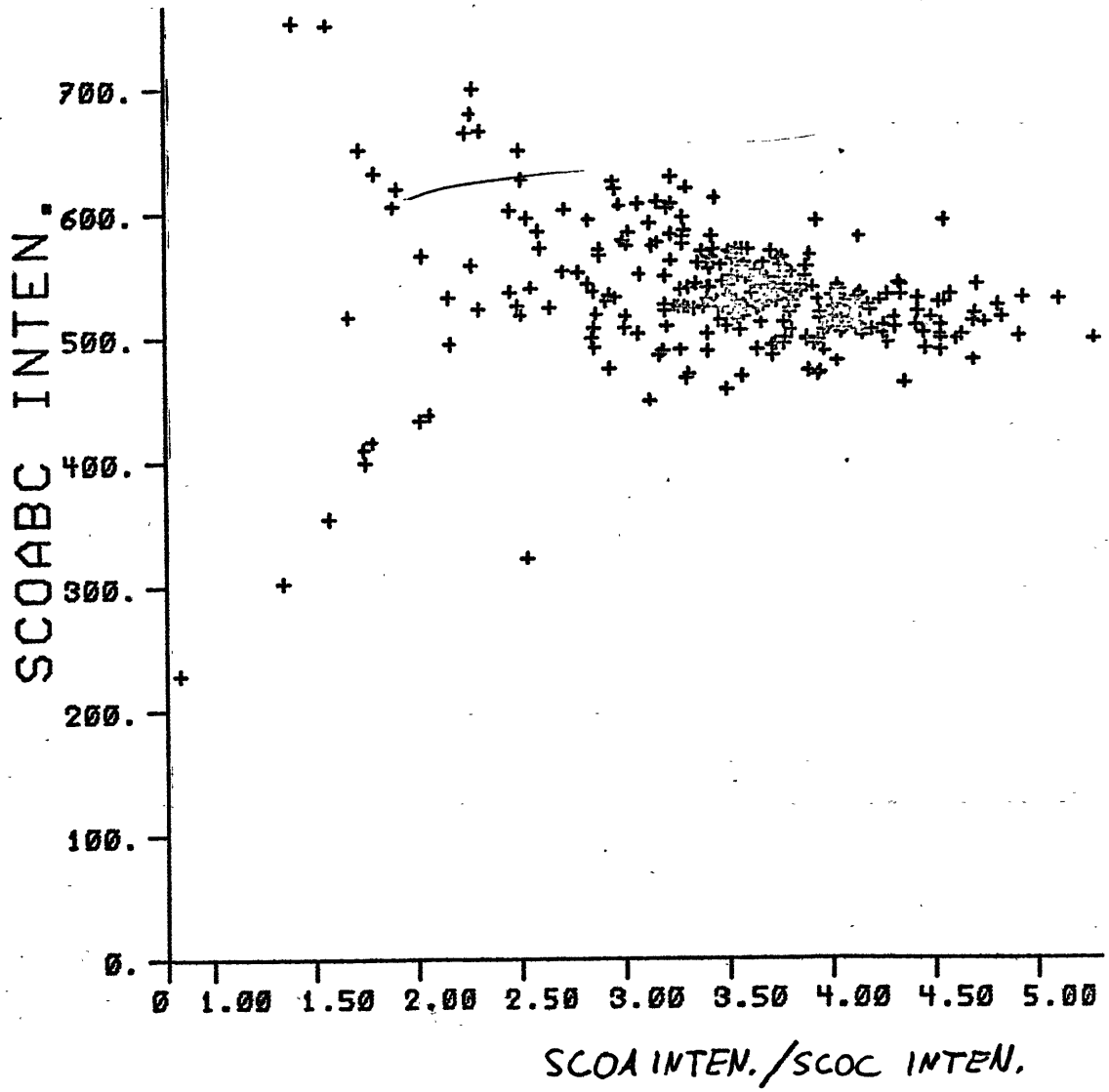Fig. 7. SCOA: SCOB Hardness Correlation.
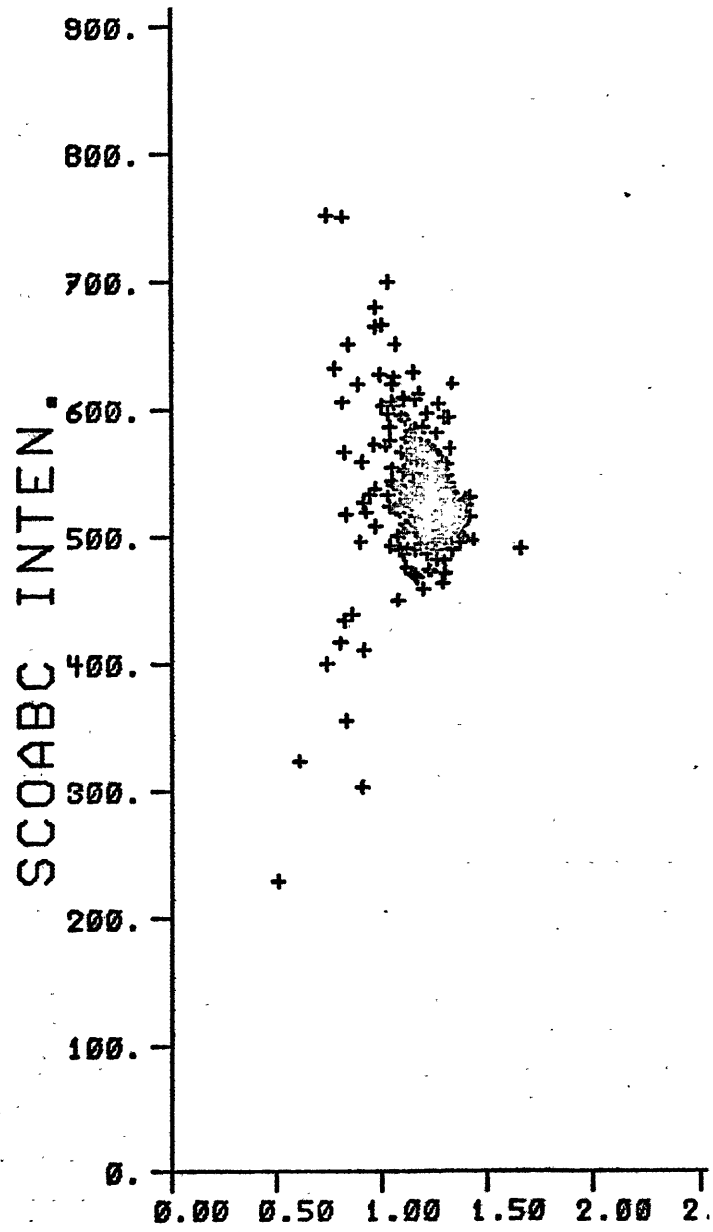
Fig, 8.   SCOA: SCOC Hardness Correlation.

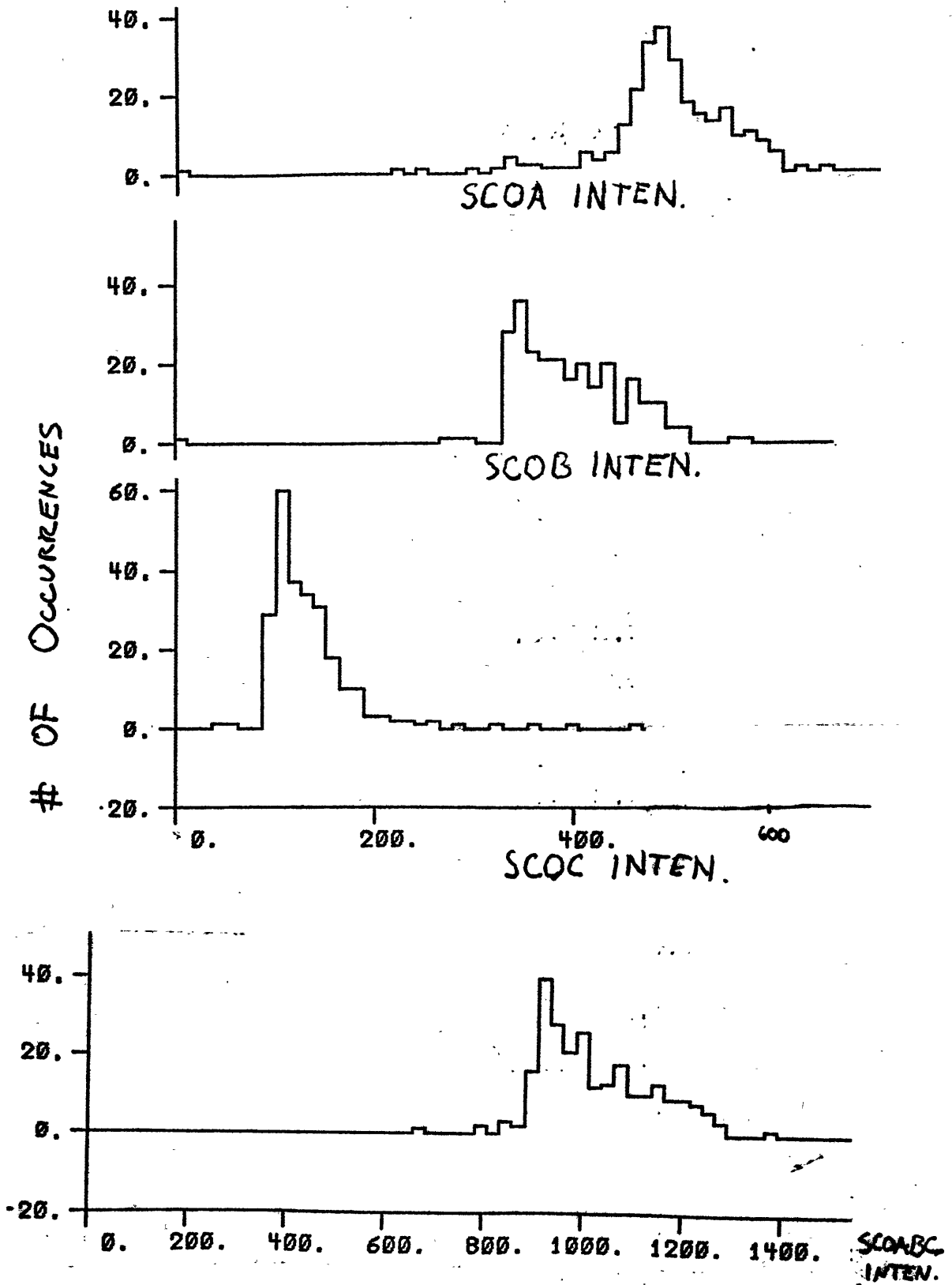Fig. 9. SCOB: SCOC Hardness Correlation.
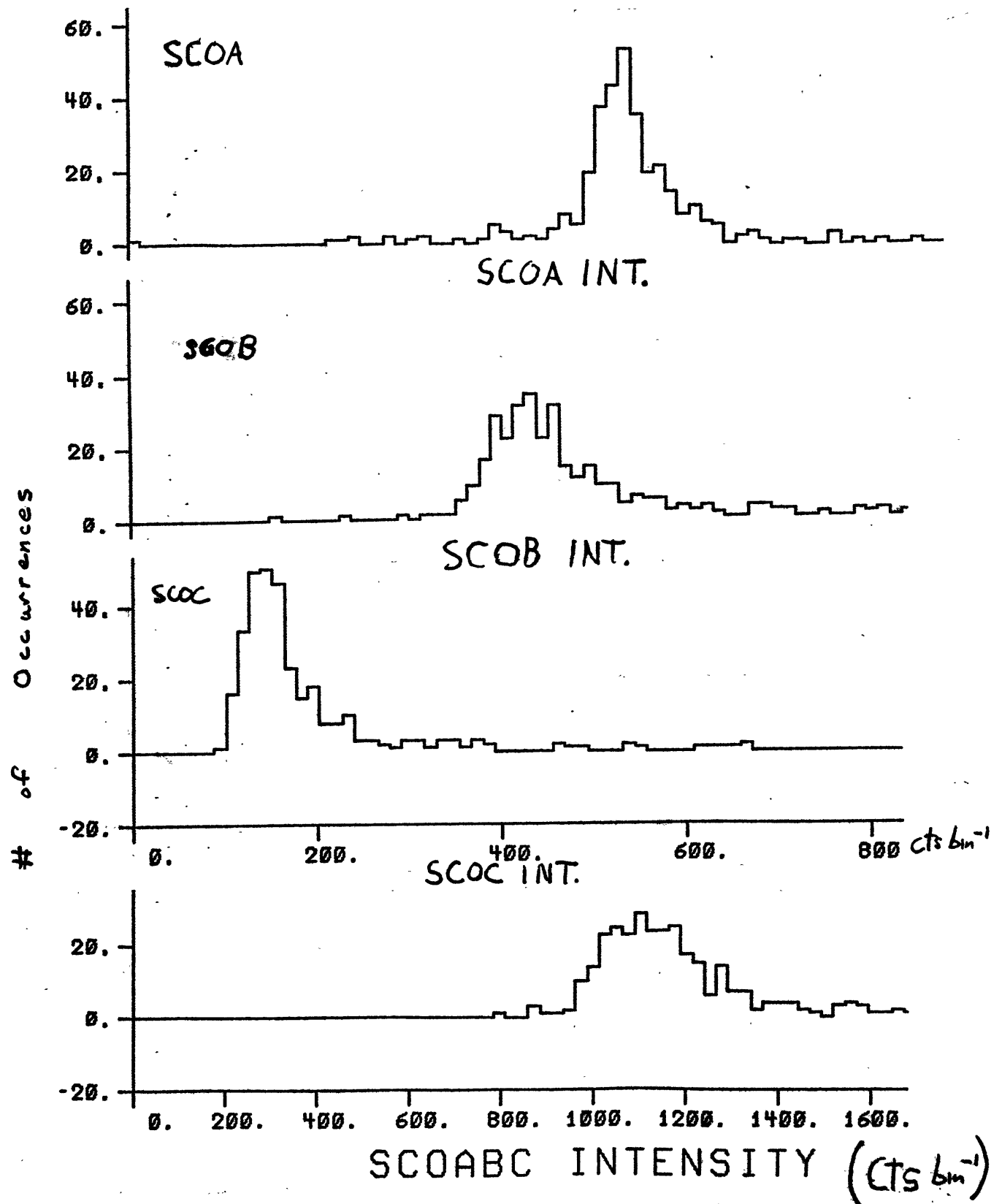
Fig. 10. Flaring Intensity Histograms.
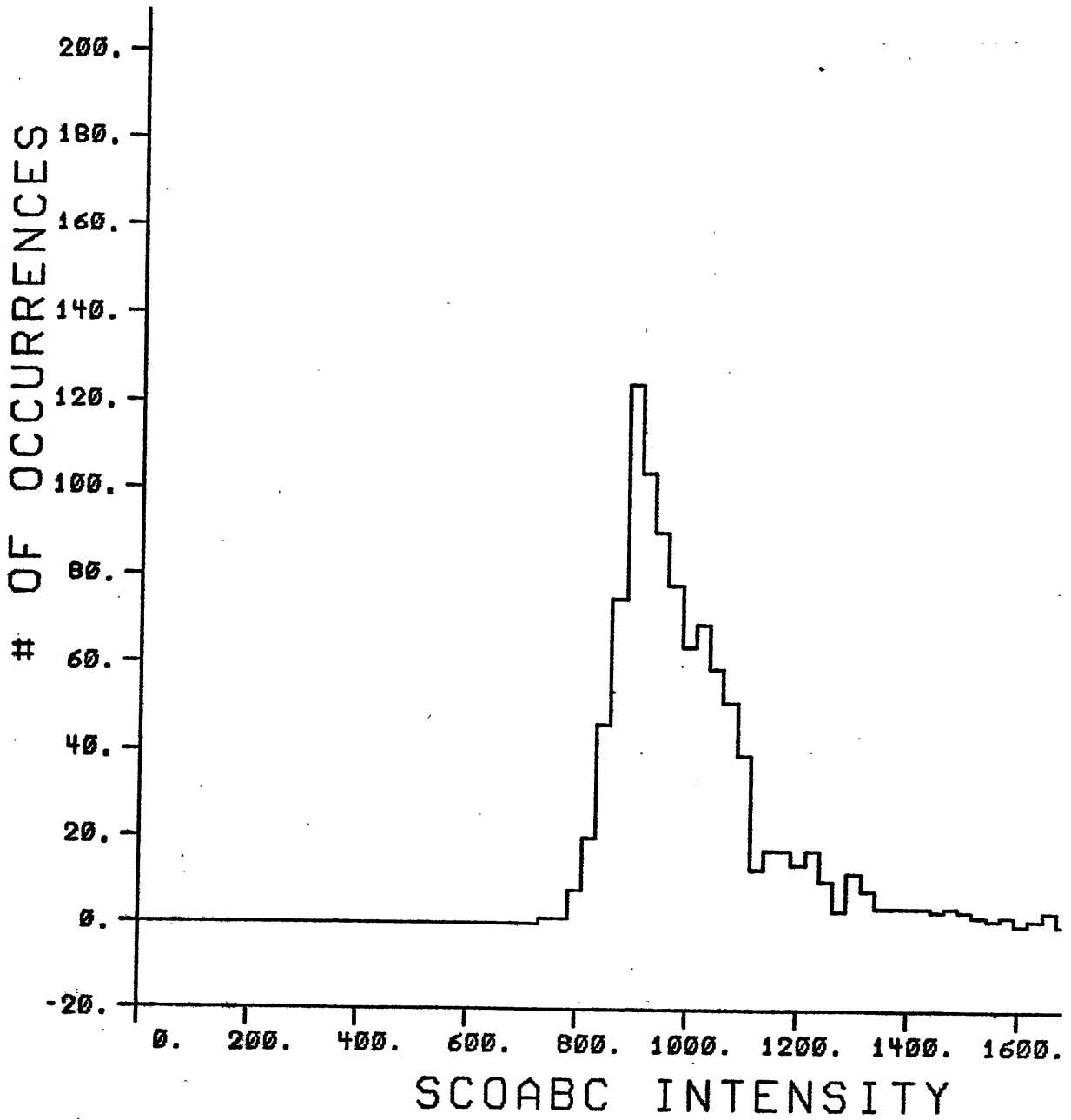
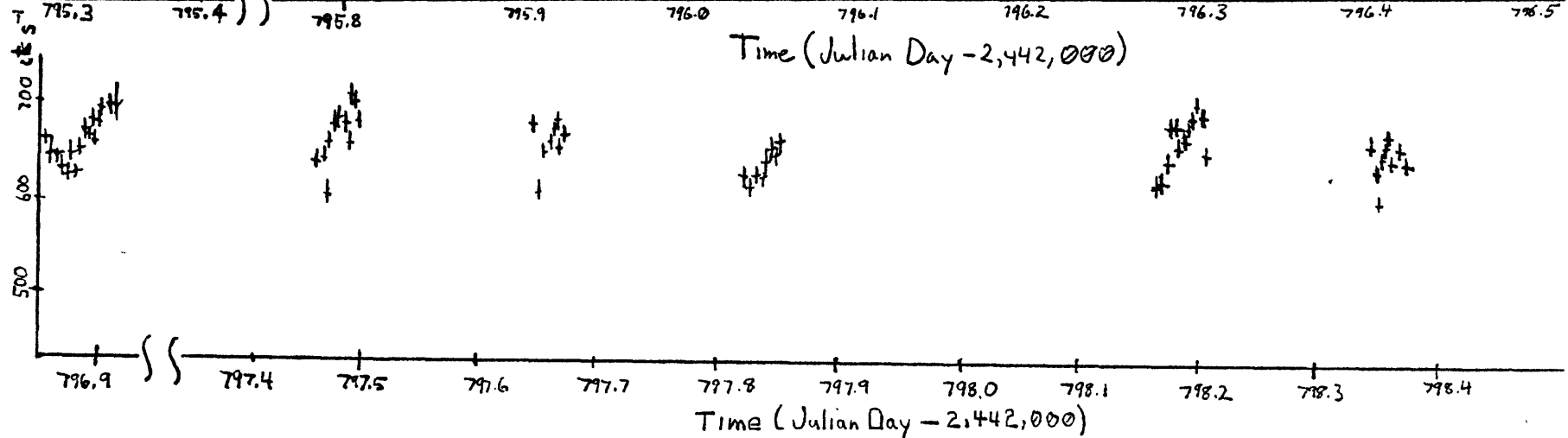Fig. 11. Quiescent Intensity Histograms.
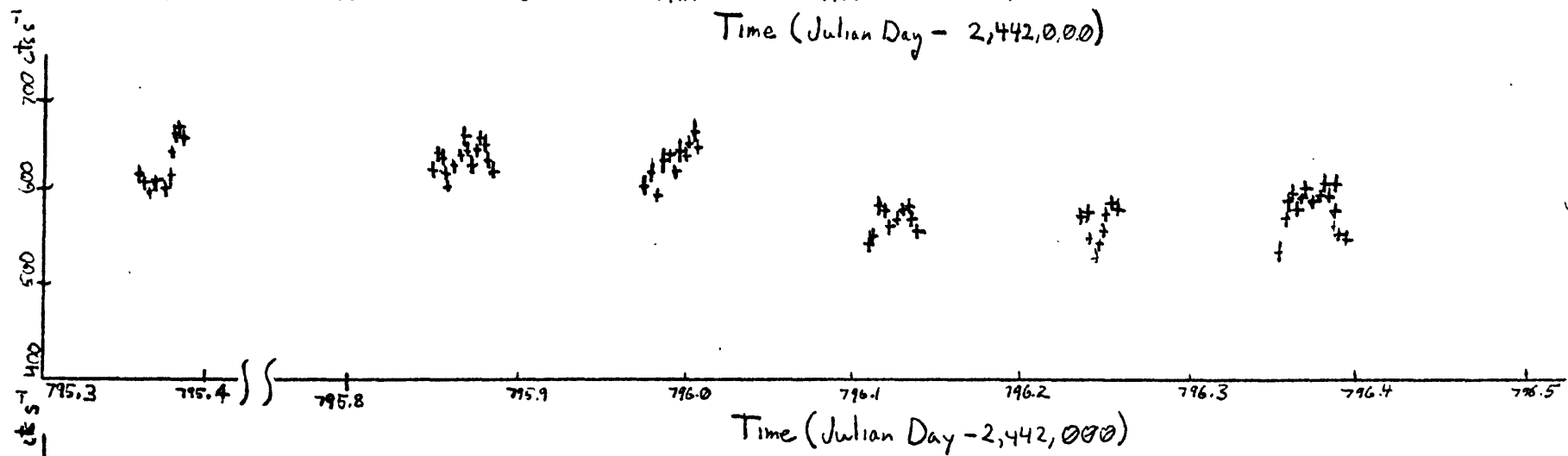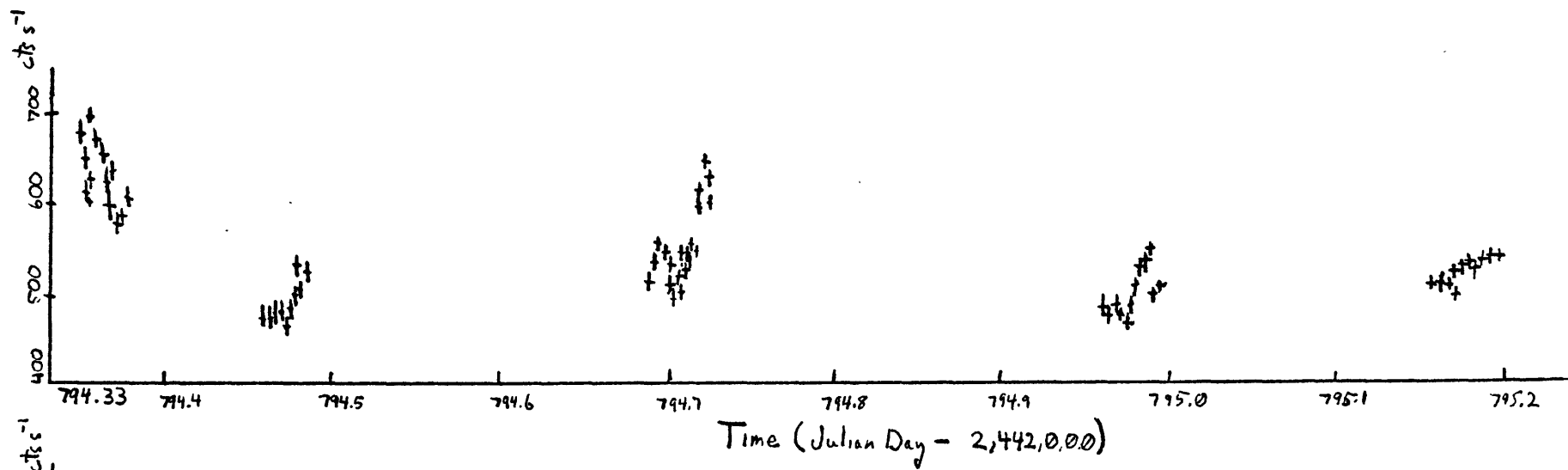
Fig. 12. High Time Resolution Intensity Histograms.
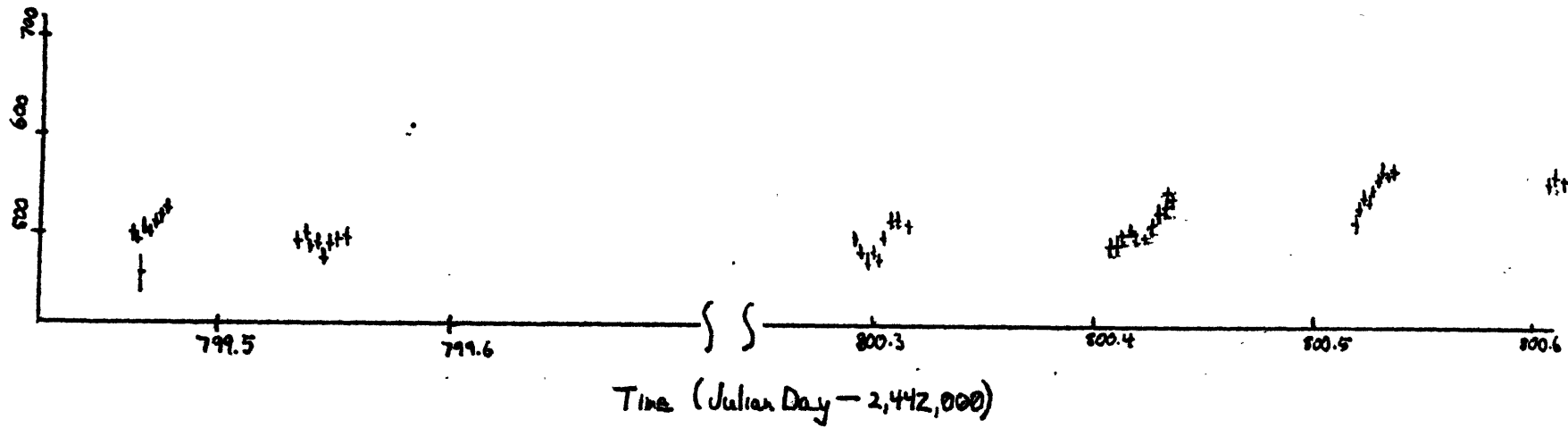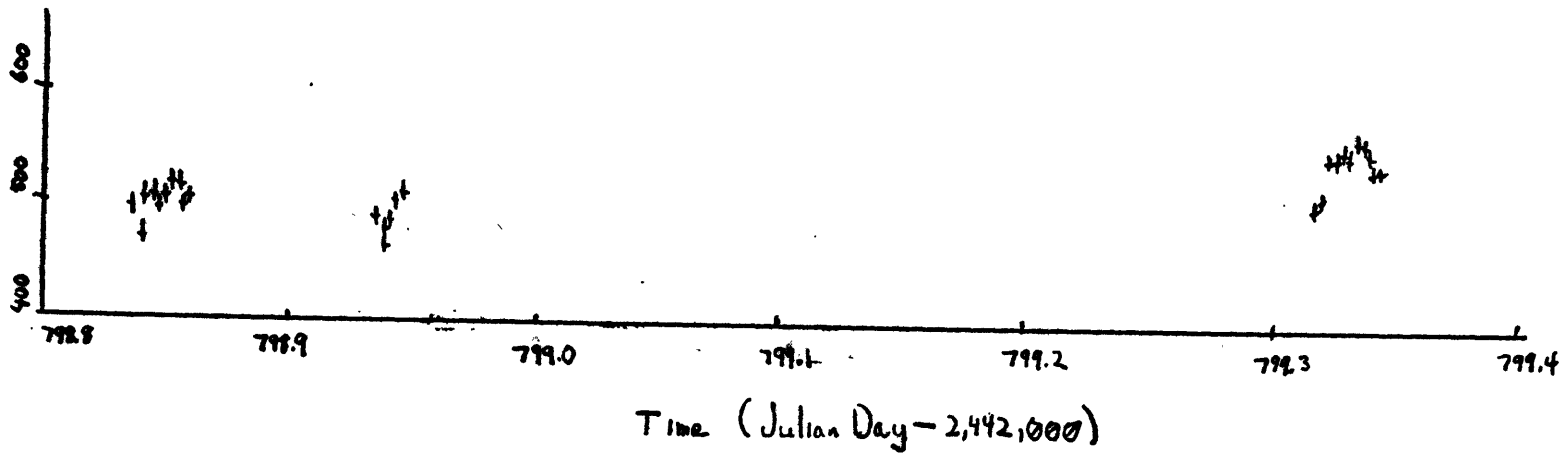
Fig. 13. Scorpio X-1 light Curve (1.0-2.5 keV).

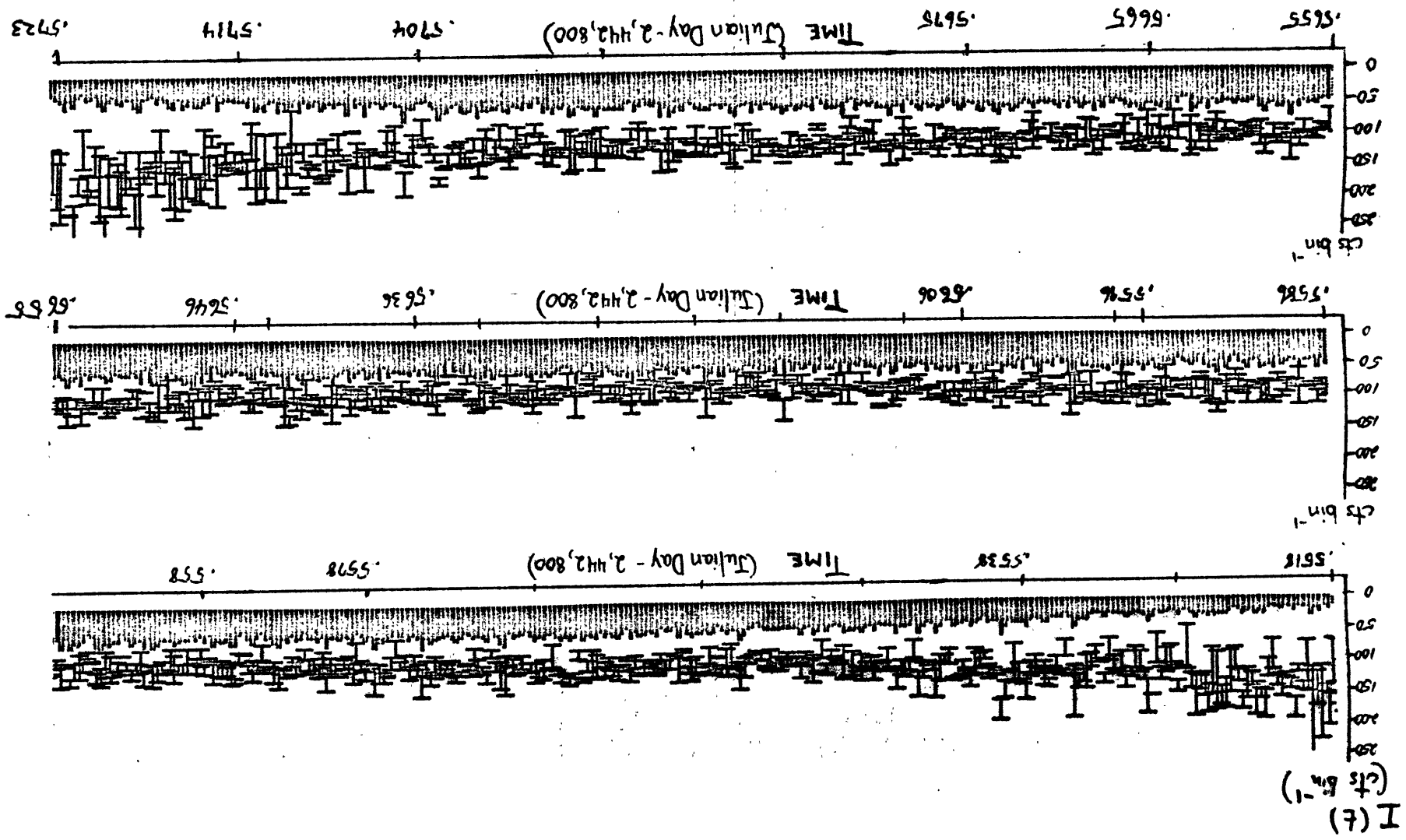Time (Julian Day — 2,442,000)

Time (Julian Day — 2,442,000)

Fig. 13. (continued)

$I(t)$

$\left(cts\ s^{-1} \times 1.663\ (= cts\ km^{-1})\right)$

Time (Julian Day − 2,442,800)

cts $s^{-1} \times 1.663$

Time (Julian Day − 2,442,800)

cts $s^{-1} \times 1.663$

Time (Julian Day − 2,442,800)
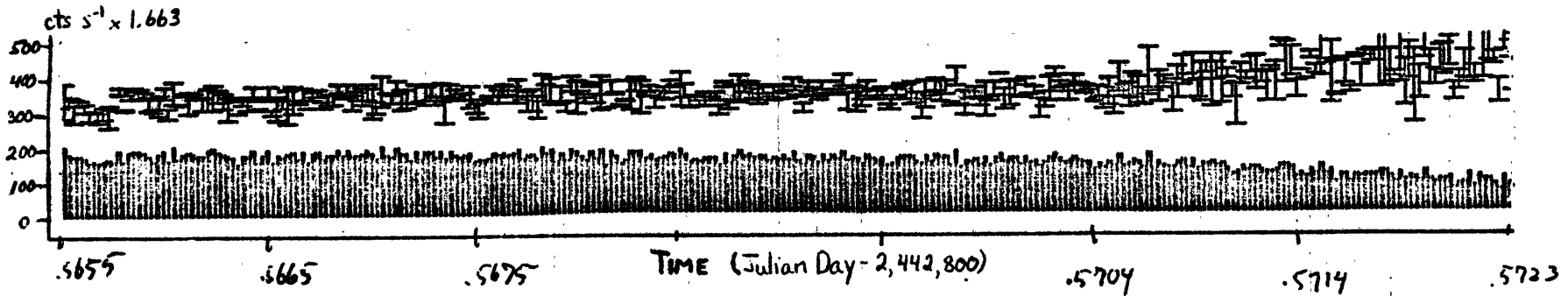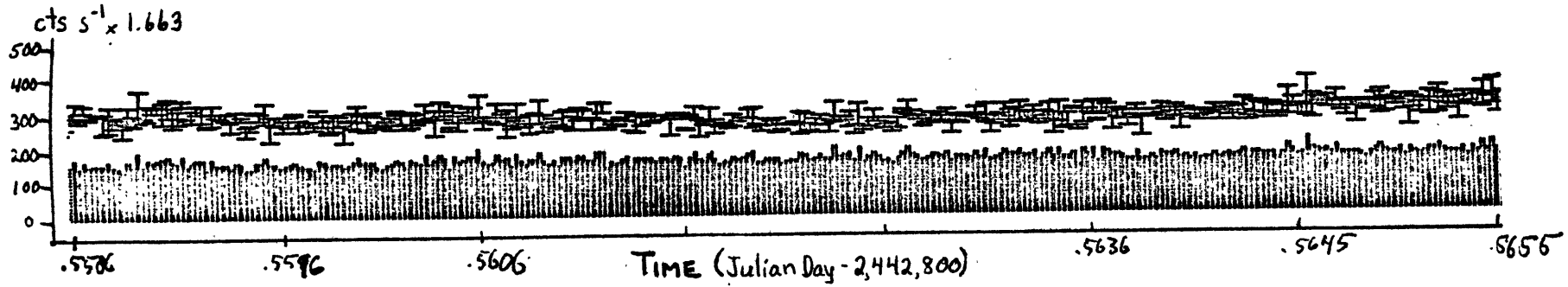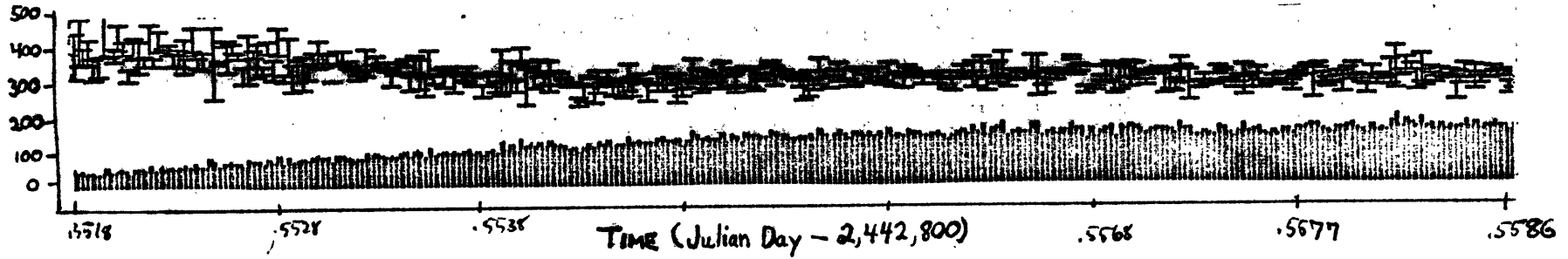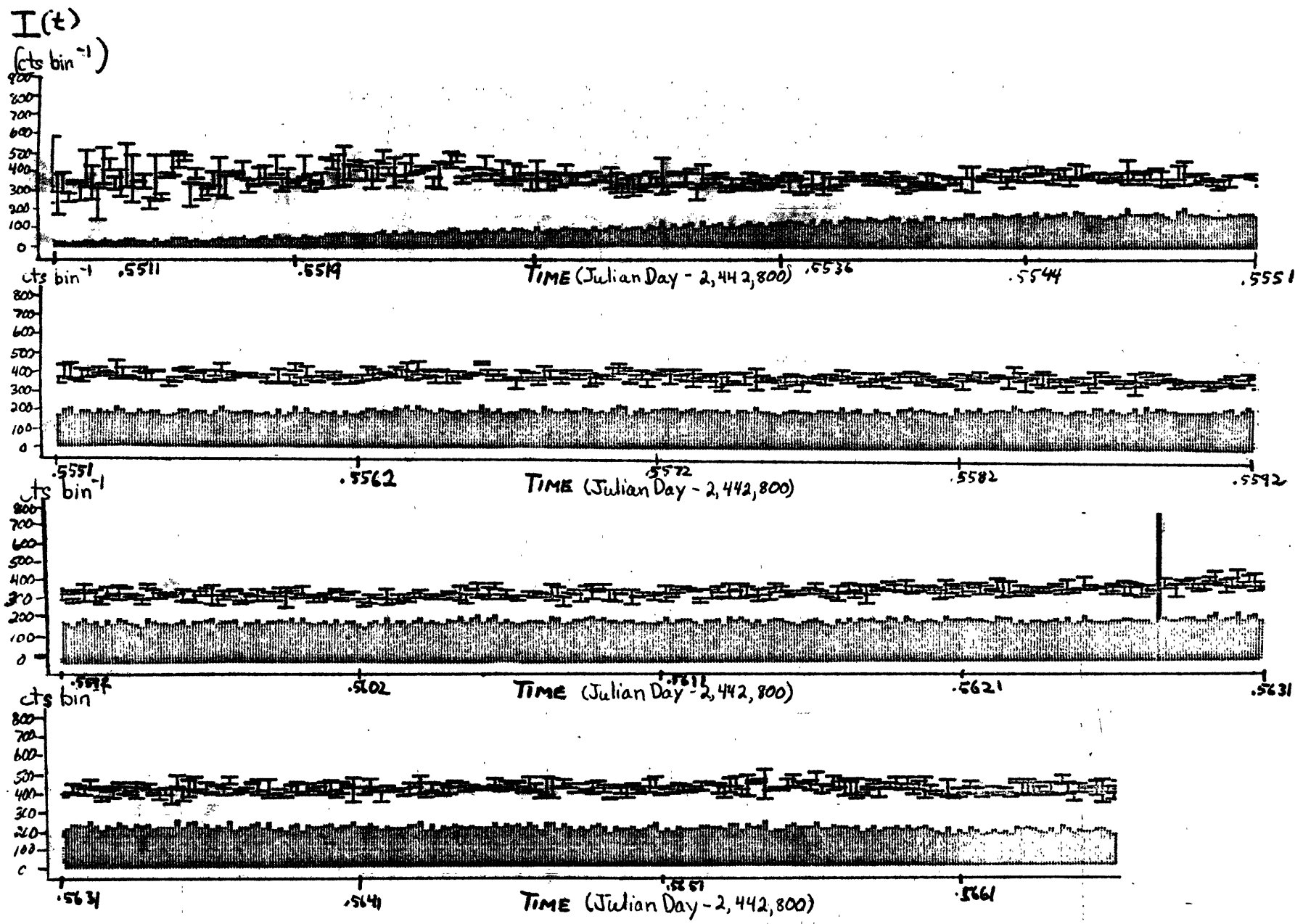
Fig. 15. 0.83 Second Time Resolution of SCOB.

Fig. 16. 0.83 Second Time Resolution of SCOA.

Although the quality of the data is not as high as could be expected, certain features stand out. The source is continuously variable (See Fig. 13). If the X-ray activity is loosely coupled to the optical, we might expect the source to be in the X-ray active state about 12% of the time, which is equivalent to three or four of the orbits analyzed. And indeed one can see that the event of Julian Day 2,442,794.35 is clearly a flare which rose. to 700 cts per sec. in a few minutes. It is followed by an orbit in which the source is at its minimum quiescent value, about 500 cts per sec. This data mimics the behavior noted by Canizares et. al. 1975. The event at day 794.70 (the first four digits will be dropped for convenience) also appears to be a flare, and is preceded and followed by low-intensity periods. At 795.2 days the source turns on into an active state, or at least a period of clearly enhanced intensity persisting for several days.

The two clear flares changed intensity by 30-40%, not very large for Sco X-1. Typical variations in a single orbit were 5-15%. The high intensity state lasted three days before falling at day 798.8. It then lay moderately quiet until day 800.4, where a gradual increase ensued which lifted the intensity by 20% over a period of five hours. All of this behavior is similar to that which was observed by Bradt et. al. 1975.

To determine whether time variation on much shorter scales could be observed, the data from day 800.55 to day 800.57 was analyzed at all three channels in time bins of .83142 seconds. The results appear in figures 14 through sixteen. It is clear from this data that substantial variations exist on time scales of as short as five seconds, and quite possibly as short as the resolution element, .83 s. In SCOC, variations of 30% are observed between successiv bins, and changes of 20-75% in from 5 to 10 seconds. In SCOB the numbers are 20% bin to bin, and 20-30% from 5 to 10 seconds. With such narrow time bins, the signal to noise ratio has dropped from circa 1000 considering all the data in a whole orbit, or circa 300 for 20 second bins (the usual si$_z$e), to about 20. The data in the highest energy channel (SCOC) appears misleadingly noisy due to the larger scale. With the 15% bin to bin variations in SCOA and its 20% changes in 5 to 10 seconds, it becomes apparent that the noise level in each channel is roughly the same, but tends to mask the lower amplitude variations in SCOC due to the relatively small intensity in that channel. Random fluctuations both inherent and background-caused should total 15 cts bin^{-1} in SCOA, 20 cts bin^{-1} in SCOB, and 24 cts bin^{-1} in SCOC (from the average background rates mentioned previously and the assumption that fluctuations add as the root mean square).

Taking these fluctuations into account, it appears
that the one bin changes are from two to three times the
expected mean fluctuation. At this level of confidence it
is not possible to definitely separate the background from
the signal in any single channel. By correlating the channels,
it should be possible to eliminate most of the noise and
enhance the source variations. When this is done, the most
noticeable effect is to bring out the 5-10 second flicker,
which appears simultaneously about 70% of the time in all
three channels, and is therefore real. The 1 bin variations
do not appear to be correlated, but that fact is most prob-
ably due to submersion in noise. Fast fourier transforms
of the data yield no period from .83142 sec to 150 sec, a
result repeated many times before by other observers. If
the flickering is powered in a similar manner to Neugebauer's
acoustically driven model, the implied order of magnitude of
the physical object responsible is on the order of 10^6 cm
for the 5-10 second flicker, and less than 10^5 cm for the
bin to bin changes, if they are real.

Examination of the intensity histogram (Fig. 10) which
was compiled at times when the source was active (high inten-
sity) reveals a much enhanced high-intensity tail, as expec-
ted, and a previously unmentioned sharp rising edge to that
histogram. This indication of a lower intensity limit while
the source is active is reminiscent of the 12.4 mag threshold

for optical flaring. The histogram in Fig. 11 portrays intensity distributions during the quiet state. It is apparent that the entire low-intensity tail is contributed during the quiet state (notwithstanding the mention by Canizares et. al. 1975 of brief, sharp dips to quiescent values during the active state, which are spaced from 20 minutes to 4 hours). The high intensity tail in this figure is much reduced and the whole envelope rounded. The mean intensity in the three channels is shifted in the active histogram relative to the quiet histogram in such a way that the spectrum during flare is a more rapidly dying exponential, ie. it gets bluer. This observation is in agreement with the statement of Canizares et. al. 1975 that Sco X-1 seems to flare stronger at higher energies.

The color-color locus of the source also changes with the activity period. During flaring, the locus of SCOA plotted against SCOB steepens, going from slope .81 to 1.0. SCOA vs. SCOC also steepens, increasing from .52 to .59 . Interestingly, the correlation coefficient for the linear regression of one intensity versus another is less for SCOA vs. SCOB during the quiescent periods, but just the opposite for SCOB vs. SCOC. If this is a real effect (the change is about 20%) it would imply slight decoupling of the various X-ray energies. If the decoupling is due to physical separation at different radii in an accretion

ring such as that in the model of Ramaty, Cheng, and Tsuruta 1974, then the radial separation has a typical length

$$r_1-r_2 = GM(E_2-E_1)/E_1E_2$$

which for M equal to one solar mass comes out to be about 2×10^8 cm. What is being implied in essence, is the condition that the gas is not entirely isothermal as in simplified models (Chodil et. al. 1968), and exhibits inhomogeneities on a scale of at least 10^8 cm.

The hardness correlation, especially in Fig. 7, indicates that the source is brighter at lower energies, a contradiction of previous deductions and observations for which no explanation is available at this time.

One additional correlation was made of orbital phase versus flare activity. From the period and minimum of Gottlieb et. al. 1975, phase zero occurs near the point 795:04 days. The two large flares which occur early in the light curve then lie near phase 0.5 and 1.0, respectively, which is suggestive but at the moment useless.

IV

CONCLUSIONS

The Scorpio Monitor Wide View Detector was given its unusually large field of view to make it effective in studies of spectral changes and temporal intensity changes. A drawback of such a wide field, however, is a formidably more complicated response function than that of narrow field detectors. Even with the response function in a crude state of approximation, however, spectral features begin to resolve themselves.

Use of all three channels as cross checks enables detection of low-amplitude fast flickering on a scale of 5 to 10 seconds. Appearance of intensity histograms is strongly dependent on the activity state of the source; when flaring or active the histogram has a high intensity tail and a well-defined low-intensity threshold. When quiescent the envelope is more slowly-varying and nearly symmetric. Color-color loci change slope according to the state of activity of the source, and a hardness: intensity correlation of some kind is strongly indicated.

LIST OF REFERENCES

Blumenthal, G. R., and Tucker, W. H. 1974. "Mechanisms for the Production of X-rays in a Cosmic Setting." In X-Ray Astronomy, pp. 99-153. Edited by R. Giacconi and H. Gursky. Astrophysics and Space Science Library Series 43. Dordrecht, Holland, and Boston: D. Reidel Publishing Company.

Bradt, H. V., Braes, L. L. E., Forman, W., Hesser, J. E., Hiltner, W. A., Hjellming, R., Kellog, E., Kunkel, W. E., Miley, G. K., Moore, G., Pel, J. W., Thomas,J., Vanden Bout, P., Wade, C., and Warner, B. 1975. The Astrophysical Journal, 197, 443.

Canizares, C. R., Clark, G. W., Lewin, W. H. G., Schnopper, H. W., and Sprott, G. F. 1973. Ap. J. (Letters), 179, L1.

Canizares, C. R., Clark, G. W., Li, F. K., Murthy, G. T., Bardas, D., Sprott, G. F., Spencer, J. H., Mook, D., Hiltner, W. A., Williams, W. L., Moffett, T. J., Grupsmith, G., Vanden Bout, P. A., Golson, J. C., Irving, C., Frohlich, A., and van Genderen, A. M. 1975. Ap. J., 197, 457.

Chodil, G., Mark, H., Rodrigues, R., Seward, F. D., Swift, C. D., Turiel, I., Hiltner, W. A., Wallerstein, G., and Mannery, E. J. 1968. Ap. J., 154, 645.

Cowley, Anne P., and Crampton, David. 1975. Ap. J. (Letters), 201, L65.

Evans, W. D., Belian, R. D., Conner, J. P., Strong, I. B., Hiltner, W. A., and Kunkel, W. E. 1970. Ap. J. (Letters), 162, L115.

Fritz, G., Meekins, J. F., Henry, R. C., Braym, E. T., and Friedman, H. 1968. Ap. J. (Letters), 153, L199.

Giacconi, R., Gursky, H., and Waters, J. R. 1965. Nature, 207, 572.

Gottleib, E. W., Wright, E. L., and Liller, W. 1974. International Astronomical Union Circular, No. 2704.

Gursky, H., and Schwartz, D. 1974. "Observational Techniques". In X-Ray Astronomy, pp. 25-98. Edited by R. Giacconi and H. Gursky. Astrophysics and Space Science Library Series 43. Dordrecht, Holland, and Boston: D. Reidel Publishing Company.

Hayakawa, S., and Matsuoka, M. 1963. Proceedings of the Conference on Cosmic Rays, Jaipur, vol. 3, 213.

Hiltner, W. A., and Mook, D. E. 1967. Ap. L., 150, 851.

Hjellming, R. M., and Wade, C. M. 1971. Ap. J. (Letters), 164, L1.

Kestenbaum, H., Angel, J. R. P., and Novick, R. 1971. Ap. J. (Letters), 164, L87.

Lewin, W. H. G., Clark, G. W., and Smith, W. B. 1968. Canadian Journal of Physics, 46, S409.

Lewin, W. H. G., Clark, G. W., and Smith, W. B. 1968. Ap. J. (Letters), 152, L55.

Li, Fuk. 1976. MIT Physics Department, Cambridge, Massachusetts. Interview, May, 1976.

Matilsky, Terry. 1975. "Detector Calibrations." SAS Memos vol. 1. Center for Space Research at the Massachusetts Institute of Technology. (Mimeographed)

McClintock, J. F., Canizares, C. R., and Tarter, C. B. 1975. Ap. J., 198, 641.

Mook, Delo E. 1967. Ap. J. (Letters), 150, L25.

Neugebauer, G., Oke, J. B., Becklin, E., and Garmire, G. 1969. Ap. J., 155, 1.

Oda, M., and Matsuoka, M. 1971. Progress in Elementary Particles and Cosmic Ray Physics, 10, 305.

Payne-Gaposchkin, C. 1957. The Galactic Novae. (Amsterdam: North Holland Publishing Company.)

Pelling, R. M. 1973. Ap. J., 185, 327.

Pringle, J. E., and Rees, M. J. 1972. Astronomy And Astrophysics, 21, 1-9.

Ramaty, R., Cheng, C. C., and Tsuruta, S. 1974. <u>Ap. J.</u>, 187, 61.

Rappaport, S., Bradt, H. V., and Mayer, W. 1969. <u>Ap. J. (Letters)</u>, 157, L21.

Rappaport, S., Bradt, H. V., Naranan, S., and Spada, G. 1969. <u>Nature</u>, 221, 428.

Rossi, B. B. 1965. "Remarks on X-Ray Astronomy". <u>Proceedings of the Solvay Institute 13th Physics Conference, Brussels, 1964</u>. (New York: Interscience Publishers).

Wade, C. M., and Hjellming, R. M. 1971. <u>Ap. J.</u>, 170, 523.

Westphal, J. A., Sandage, A., and Kristian, J. 1968. <u>Ap. J.</u>, 154, 139.